SLAC-181
UC-34d
(E)

AN EXPERIMENTAL STUDY OF THE DECAY $K_L^o \to \pi^+\pi^-\pi^o$ *

DAVID NEIL SLONE

STANFORD LINEAR ACCELERATOR CENTER
STANFORD UNIVERSITY
Stanford, California 94305

PREPARED FOR THE U.S. ATOMIC ENERGY
COMMISSION UNDER CONTRACT NO. AT(04-3)-515

Manuscript Completed August 1974

Printed in the United States of America. Available from National Technical Information Service, U.S. Department of Commerce, 5285 Port Royal Road, Springfield, VA 22161. Price: Printed Copy $6.25; Microfiche $1.45.

*Ph.D. dissertation.

AN EXPERIMENTAL STUDY OF THE DECAY K-ZERO-LONG ----> PI-PLUS PI-MINUS PI-ZERO

A 2-meter streamer chamber was located in the neutral 5 degree beam at the Stanford Linear Accelerator Center (SLAC) and was triggered on K-zero-long decays. During 1158 hours of running between July and October of 1970, approximately 2,500,000 events were photographed, 500,000 of which were K-zero-long decays. The principal charged decay modes of the K-zero-long are:

K-zero-long ----> pi-plus pi-minus pi-zero (K3pi)
K-zero-long ----> pi-plus-minus mu-minus-plus neutrino (Kmu3)
K-zero-long ----> pi-plus-minus e-minus-plus neutrino (Ke3)

This report presents an analysis of the purely hadronic K3pi mode based on 20% of the total sample (100,000 K-zero-long decays).

Many earlier experiments in the field suffered from systematic biases which necessitated large (and possibly poorly understood) corrections to the data. The resultant confusion pointed to the need for a reasonably high statistics experiment which was not dominated by systematic errors. This experiment was designed to be almost free of systematic biases so that the corrections to the data were at the 2% level. The main experimental features are described below.

a) An extremely favorable geometric configuration resulted in a trigger efficiency which exceeded 98% over the entire Dalitz plot. The scanning efficiency was estimated to be in excess of 99.5%.

b) The time-of-flight of the K-zero-long was determined with an average error of ±0.45 ns. This was incorporated with the track measurements on film into a one constraint (1C) kinematic fit, resulting in a very clean separation of the decay modes.

c) Shower plates inside the chamber allowed a partial identification of the K-zero-long decay products. This served as an independent check on the kinematic fit.

The decay spectrum was found to depend on the pi-zero center-of-mass kinetic energy (T3) in a manner well described by a matrix element of the form

M(+ - 0) = a (1 + b(2(T3)-T3max)/T3max)

where the value of b was determined to be -0.443 ± 0.014 . A comparison with K-plus decays shows a significant violation of the delta I=1/2 rule for hadronic weak decays.

ACKNOWLEDGEMENTS

I am pleased to thank all of the people who worked closely with me during the course of this experiment.

The experiment was a collaboration between SLAC and Brookhaven. One fifth of the data was analyzed at SLAC and is the subject of this report. The rest is currently being analyzed at Brookhaven by Mark Sakitt, Glen Snape, and Allen Stevens. My involvement with the Brookhaven collaborators was mainly during the data acquisition in which Mark Sakitt, David Hill, Joshua Kopp, and Julia Thompson participated. Mark and I have subsequently conferred on many occasions regarding our respective progress in analyzing the data.

The streamer chamber and all the peripheral equipment (including the magnet, camera system, gas system, etc.) was the responsibility of many people. Boris Bertolucci, Jobst Brandt, Vernon Lee, Earl Maninger, John McKee, Edward McNerney, James Moss, Franz Plunder, Tom Pulliam, Gerhardt Schultz, Leroy Schwarcz, and William Wadley were involved in various aspects of the planning and construction as well as in the day-to-day running and maintenance of the equipment.

The beam was designed by Joseph Murray and Robert Vetterlein while the accelerator staff had the difficult job of delivering a "beam knockout" beam for many hours.

Florence Shuster and many members of CDA helped in the data analysis, and Phyllis Jairl assisted in many ways.

The members of the SLAC Streamer Chamber Group mentioned below were involved in the experimental running, and working with them was a most enjoyable experience. The individual references are not meant to define the scope of each person's involvement in the experiment except as it related to my work.

Professor Robert Mozley, my thesis advisor, has treated me with respect and has shown great interest in my problems and ideas. I appreciate this deeply.

Kirk Bunnell, who supervised the construction of the streamer chamber, showed that it was possible to build a chamber that would last 2,500,000 shots. This was crucial to the experiment. I had the pleasure of working with William Swanson and Fook Fah Liu supervising the scanning and measuring. Fook Fah Liu also helped me greatly with the Monte Carlo studies. Francesco Villa and Allen Odian always had valuable suggestions to make. I learned from them that nothing is negligible a priori. Many small effects that had been ignored were subsequently found to require attention.

The two people I worked with most closely were Lichen Wang and Joseph Park. Lichen and I wrote the geometry and optical constants programs together, and the valuable lesson imparted was that many things are more easily done than said. Joseph and I worked on the kinematic fitting and timing constants determination. I got my first glimpse of truly elegant programming and began to learn the fine art of programming with an eye to the future.

Professor David Hitlin of the Stanford Physics Department acted as co-signer for this thesis and I welcomed his useful comments and discussions. Special thanks are due Robert Messner of the University of Colorado who patiently explained many of the intricacies of radiative corrections and provided the necessary Fortran code.

TABLE OF CONTENTS

LIST OF TABLES

LIST OF FIGURES

INTRODUCTION

A 2-meter streamer chamber was located in the neutral 5° beam at the Stanford Linear Accelerator Center (SLAC) and was triggered on K^0_L decays. During 1158 hours of running between July and October of 1970, approximately 2,500,000 events were photographed, 500,000 of which were K^0_L decays. The principal charged decay modes of the K^0_L are:

$K^0_L \longrightarrow \pi^+\pi^-\pi^0$ (K3pi or 3 pi)

$K^0_L \longrightarrow \pi^\pm\mu^\mp\nu$ (Kmu3)

$K^0_L \longrightarrow \pi^\pm e^\mp\nu$ (Ke3)

This report presents an analysis of the purely hadronic decay mode $K^0_L \longrightarrow \pi^+\pi^-\pi^0$ based on 20% of the total sample (100,000 K^0_L decays).

Many earlier experiments in the field suffered from systematic biases which necessitated large (and possibly poorly understood) corrections to the data. The resultant confusion pointed to the need for a reasonably high statistics experiment which was not dominated by systematic errors. This experiment was designed to be almost free of systematic biases so that the corrections to the data were at the 2% level. The main experimental features are described below.

a) An extremely favorable geometric configuration resulted in a trigger efficiency which exceeded 98% over the entire Dalitz plot. The scanning efficiency was estimated to be in excess of 99.5%.

b) The time-of-flight of the K^0_L was determined with an average error of ±0.45 ns. This was incorporated with the track measurements on film into a one constraint (1C) kinematic fit, resulting in a very clean separation of the decay modes.

c) Shower plates inside the chamber allowed a partial identification of the K^0_L decay products. This served as an independent check on the kinematic fit.

The decay spectrum was found to depend on the π^0 center-of-mass kinetic energy (T3) in a manner well described by a matrix element of the form

$$M(K^0_L \longrightarrow \pi^+\pi^-\pi^0) \sim 1 + \sigma\,(2(T3)-T3max)/T3max$$

where the value of σ was determined to be -0.443 ± 0.014 . A comparison with K+ decays shows a significant violation of the $\Delta I=1/2$ rule.

CHAPTER I

THEORETICAL CONSIDERATIONS

The 3 pi decay of the K^0_L is interesting because a comparison with the 3 pi decays of the charged K's gives information about the isospin transitions in nonleptonic weak interactions. A general discussion of the $\Delta I=1/2$ rule is given below, followed by a detailed isospin analysis of K--->3 pi decays.

HADRONIC WEAK DECAYS AND THE $\Delta I=1/2$ RULE

Of the many known weak decays, the least understood is the class of strangeness-changing purely hadronic decays. In fact, the selection rules governing these decays are not known with certainty, much of the uncertainty revolving about the so-called $\Delta I=1/2$ rule. I is the total isotopic spin of the system, and the rule states that the magnitude of the change of I is 1/2.

The rule was postulated by Pais and Gell-Mann in 1955[1] as part of the ongoing effort to systematize the mcunting body of observed weak decays. A less stringent form of the rule, namely $|\Delta I^3|=1/2$ where I^3 is the third component of the total isospin I, was first put forth by Pais. This is equivalent to the relation $Q = I^3 + (B+S)/2$ coupled with the well-established conservation of charge and baryon number and the apparent non-existence of transitions with $|\Delta S|>1$. The more restrictive $\Delta I=1/2$ rule was offered by Gell-Mann as a further speculation.

1. Evidence for the $\Delta I=1/2$ Rule - Two Pion Decays

The oft-cited evidence for the near validity of the $\Delta I=1/2$ rule is the suppression of the decay $K^+ \longrightarrow \pi^+\pi^0$ relative to the decays $K^0_S \longrightarrow \pi^+\pi^-$ and $K^0_S \longrightarrow \pi^0\pi^0$ (2). Treating the pions as identical bosons dictates a total

state which is symmetric with respect to interchange of the pions. Since the K and the π are spinless, the pion pair must be in an S state (spatially symmetric), hence the isospin state must be symmetric as well. It is then easily seen that there is only one possible final state for the pions in each of the three decays. The states are:

$$\sqrt{1/2}\ (\,|{+0}\rangle + |{0+}\rangle\,) = |2,1\rangle \quad \text{for } K^+ \longrightarrow \pi^+\pi^0,$$

$$\sqrt{1/2}\ (\,|{+-}\rangle + |{-+}\rangle\,) = \sqrt{1/3}\ |2,0\rangle + \sqrt{2/3}\ |0,0\rangle \quad \text{for } K^0_S \longrightarrow \pi^+\pi^-, \text{ and}$$

$$|00\rangle = \sqrt{2/3}\ |2,0\rangle - \sqrt{1/3}\ |0,0\rangle \text{ for } K^0_S \longrightarrow \pi^0\pi^0.$$

where:

$|ij\rangle$ is the state where pions 1 and 2 have I^3= i and j respectively (note that $\pm$ means ± 1), and

$|I,I^3\rangle$ is the two pion state in terms of the total isospin.

Since the K has isospin 1/2, it is evident that to end up in the pure I=2 state, $K^+ \longrightarrow \pi^+\pi^0$ must occur via $\Delta I=3/2$ or $\Delta I=5/2$. The fact that this decay goes some 500 times more slowly than the K^0_S decays indicates the suppression of $\Delta I>1/2$ transitions relative to $\Delta I=1/2$ transitions. The observed rate is actually too high to be due to electromagnetic breaking of a strict $\Delta I=1/2$ rule, as the suppression would then be by a factor of 10^4.

2. Weak Currents

The "current-current" interaction has proved to be a useful form for expressing the effective Lagrangian of all weak processes.

$L \sim (J^{\mu})^{\dagger} J_{\mu}$

$J = J(\text{hadronic}) + j(\text{leptonic})$

$J(\text{hadronic}) = J(\Delta S=0) + J(\Delta S=1)$

where:

L is the effective Lagrangian,

J is the total weak current composed of a hadronic and a leptonic part, and

$J(\Delta S=0)$, $J(\Delta S=1)$ are the strangeness-conserving and the strangeness-changing parts of the hadronic current.

Thus the Lagrangian contains terms responsible for leptonic, semileptonic, and nonleptonic decays. The latter is the quantity of interest here and is given by:

$L(\text{nonleptonic}) \sim (J^{\mu}(\Delta S=0))^{\dagger} J_{\mu}(\Delta S=1) + \text{h.c.}$

Since $J(\Delta S=0)$ is an isovector and $J(\Delta S=1)$ is an isospinor, L(nonleptonic) contains in general a $\Delta I=3/2$ part as well as a $\Delta I=1/2$ part. A strict $\Delta I=1/2$ rule can be built into the theory by introducing neutral currents[3]. Since neutral strangeness-changing lepton currents do not appear to exist, the prospect of neutral strangeness-changing hadron currents is considered unpleasant by many as it destroys the analogy between the leptonic and hadronic realms.

Another approach is to assume conditions whereby the dynamics enhance the transitions with $\Delta I=1/2$ relative to those with $\Delta I>1/2$. Soft pion calculations make use of PCAC and current commutation relations to make statements about matrix elements at unphysical points. For $K \longrightarrow 3\pi$, it can be shown[4,5] that at the point where the pion 4-momenta vanish, a rigorous $\Delta I=1/2$ rule holds. If the extrapolation back onto the mass shell is in some sense smooth, an approximate $\Delta I=1/2$ rule can be expected to hold for the physical process. Callen and Treiman showed[6] that the matrix element for $K^0_L \longrightarrow \pi^+\pi^-\pi^0$ vanishes in the limit of vanishing π^+ (or π^-) 4-momentum.

Empirically it is known that the matrix element M(+-0) is approximately linear in the π^0 kinetic energy. We define Lorentz scalars s0, s1, s2, and s3 by:

$si = (P0-pi)^2$ for i=1,2,3, and

$3(s0) = s1 + s2 + s3 = M0^2 + m1^2 + m2^2 + m3^2$

where:

P0 is the K 4-momentum,

p1,p2,p3 are the pion 4-momenta, and

M0,m1,m2,m3 are the masses of the K and the pions.

Calculating in the c.m. gives:

$si = (M0-mi)^2 - 2(M0)(Ti)$ for i=1,2,3

where Ti is the c.m. kinetic energy of pion #i. If pion #3 is the π^0, $M(+-0) \sim 1 + \sigma(s3-s0)$ where σ is the so-called slope parameter. The extrapolation to zero 4-momentum gives a value of $.24/m(\pi^+)^2$ which is within 25% of the experimental result.

The next section considers the detailed isospin structure of the matrix element for $K \longrightarrow 3\pi$ and indicates how the $\Delta I=1/2$ rule can be tested in these decays.

ISOSPIN ANALYSIS OF 3 PI DECAYS

The early analysis by Dalitz[7] made the prediction that the ratio of the rates of $K^+ \longrightarrow \pi^+\pi^+\pi^-$ and $K^+ \longrightarrow \pi^+\pi^0\pi^0$ was 4 after phase space corrections had been made. The result depended not on $\Delta I=1/2$, but rather on the final state's having I=1. Assuming a final state of isospin 1, the relative rates of $K^0_L \longrightarrow 3\pi$ and $K^+ \longrightarrow 3\pi$ were shown to be sensitive to the amount of $\Delta I=3/2$ admixture, while the relative rates of $K^0_L \longrightarrow 3\pi^0$ and $K^0_L \longrightarrow \pi^+\pi^-\pi^0$ were insensitive. The ratio of the latter two rates corrected for phase space differences was predicted to be 1.5. None of the above considerations made any explicit reference to the energy dependence of the decay matrix element.

Weinberg[8] then showed that a comparison of the energy spectra of the odd pion in the decays $K^+ \longrightarrow \pi^+\pi^+\pi^-$ and $K^+ \longrightarrow \pi^+\pi^0\pi^0$ provided a test of the $\Delta I=1/2$ rule. Dalitz's result on the branching ratio of these two decay modes was also obtained.

The paper of Barton, Kacser, and Rosen[9] provided a rather complete isospin analysis of $K \longrightarrow 3\pi$. Since Dalitz's and Weinberg's results are included in their treatment, a detailed outline of the paper is given below.

1. The Isospin States

The first step involves writing down the eigenstates of total isotopic spin for the three pions. Combining the isospins of the first two pions to get a total isospin of I^{12}, and then combining this with the third pion's isospin gives a state denoted by $|I^{12},I,I^3\rangle$ where I^3 is the 3^{RD} component of I. I^3 is 0 for K^0 decays and ± 1 for K^+ and K^- decays. In all there are seven such states for the K^0 decay, six for the K^+ (no $I=0$ state since $I^3=1$).

The K^0 isospin states are:

$$\begin{aligned} |1,0,0\rangle = \sqrt{1/6}\ (\ &|{+}0{-}\rangle + |0{-}{+}\rangle + |{-}{+}0\rangle \\ &- |{-}0{+}\rangle - |0{+}{-}\rangle - |{+}{-}0\rangle\ ) \end{aligned}$$

$$\begin{aligned} |0,1,0\rangle &= \sqrt{1/3}\ (\ |{+}{-}0\rangle + |{-}{+}0\rangle - |000\rangle\ ) \\ |1,1,0\rangle &= (1/2)(\ |{+}0{-}\rangle + |{-}0{+}\rangle - |0{+}{-}\rangle - |0{-}{+}\rangle\ ) \\ |2,1,0\rangle &= \sqrt{1/60}\ \{\ 3(|{+}0{-}\rangle + |{-}0{+}\rangle + |0{+}{-}\rangle + |0{-}{+}\rangle) \\ &\qquad - 2(|{+}{-}0\rangle + |{-}{+}0\rangle) - 4|000\rangle\ \} \end{aligned}$$

$$\begin{aligned} |1,2,0\rangle &= \sqrt{1/12}\ (\ |{+}0{-}\rangle + |0{-}{+}\rangle + 2|{+}{-}0\rangle \\ &\qquad - |{-}0{+}\rangle - |0{+}{-}\rangle - 2|{-}{+}0\rangle\ ) \\ |2,2,0\rangle &= (1/2)(\ |{+}0{-}\rangle + |0{+}{-}\rangle - |{-}0{+}\rangle - |0{-}{+}\rangle\ ) \end{aligned}$$

$$\begin{aligned} |2,3,0\rangle = \sqrt{1/10}\ (\ &|{+}0{-}\rangle + |{-}0{+}\rangle + |0{+}{-}\rangle + |0{-}{+}\rangle + |{+}{-}0\rangle + |{-}{+}0\rangle \\ &+ 2|000\rangle\ ) \end{aligned}$$

The K^+ isospin states are:

$$\begin{aligned} |0,1,1\rangle &= \sqrt{1/3}\ (\ |{+}{-}{+}\rangle + |{-}{+}{+}\rangle - |00{+}\rangle\ ) \\ |1,1,1\rangle &= (1/2)(\ |{-}{+}{+}\rangle - |{+}{-}{+}\rangle + |{+}00\rangle - |0{+}0\rangle\ ) \\ |2,1,1\rangle &= \sqrt{1/60}\ [\ |{+}{-}{+}\rangle + |{-}{+}{+}\rangle + 6|{+}{+}{-}\rangle \\ &\qquad - 3(|{+}00\rangle + |0{+}0\rangle) + 2|00{+}\rangle\ ] \end{aligned}$$

$$\begin{aligned} |1,2,1\rangle &= (1/2)(\ |{+}{-}{+}\rangle - |{-}{+}{+}\rangle + |{+}00\rangle - |0{+}0\rangle\ ) \\ |2,2,1\rangle &= \sqrt{1/12}\ (\ 2|{+}{+}{-}\rangle - |{+}{-}{+}\rangle - |{-}{+}{+}\rangle \\ &\qquad + |{+}00\rangle + |0{+}0\rangle - 2|00{+}\rangle\ ) \end{aligned}$$

$$\begin{aligned} |2,3,1\rangle = \sqrt{1/15}\ [\ &|{+}{+}{-}\rangle + |{+}{-}{+}\rangle + |{-}{+}{+}\rangle \\ &+ 2(|{+}00\rangle + |0{+}0\rangle + |00{+}\rangle)\ ] \end{aligned}$$

To introduce energy dependence into the final states we use the Lorentz scalars s0, s1, s2, and s3 defined in the previous section. Since only two of the si are independent, one formulates the problem hereafter in terms of (s3-s0) and (s2-s1) which correspond closely to the Dalitz plot variables defined in a later chapter.

The requirement is now introduced that the final state of the three pions be totally symmetric with respect to interchange of isospin and energy variables of any two pions, and that the dependence on the variables (s3-s0) and (s2-s1) be at most linear. The result of straightforward algebraic manipulation leads to four possible states:

$|1,I^3(S)\rangle = \sqrt{5/9}\ |0,1,I^3\rangle + \sqrt{4/9}\ |2,1,I^3\rangle$

$|3,I^3(S)\rangle = |2,3,I^3\rangle$

$$|1,I^3(L)\rangle = \{\sqrt{4/9}\ |0,1,I^3\rangle + \sqrt{5/9}\ |2,1,I^3\rangle\}(s3-s0) + \sqrt{1/3}\ |1,1,I^3\rangle(s2-s1)$$

$$|2,I^3(L)\rangle = |2,2,I^3\rangle(s3-s0) + \sqrt{1/3}\ |1,2,I^3\rangle(s2-s1)$$

$|I,I^3(X)\rangle$ is the state of total isospin I and third component I^3 (0 or 1 for K^0 or K^+). X refers to the dependence on the energy variables - S for independent, L for linearly dependent.

2. Transition Matrix Elements and Predictions

The final state for K^+ decay can be written:

$$|f\rangle = a^+(1,S)|1,1(S)\rangle + a^+(1,L)|1,1(L)\rangle + a^+(2,L)|2,1(L)\rangle$$
$$a^+(3,S)|3,1(S)\rangle$$

where:

$a^+(I,X) = \langle I,1(X)|H'|K^+\rangle$, and

H' is the weak interaction Hamiltonian.

The transition matrix elements for the final states $|{+}{+}{-}\rangle$ and $|00{+}\rangle$ are obtained by using the explicit wave functions and evaluating $\langle{+}{+}{-}|f\rangle$ and $\langle 00{+}|f\rangle$. If M(abc) is the matrix element in question, we have:

$$M(++-) = (\sqrt{4/15}\ a^+(1,S) + \sqrt{1/15}\ a^+(3,S)) - \sqrt{1/3}\ (a^+(1,L) - a^+(2,L))(s3-s0)$$

$$M(00+) = (-\sqrt{1/15}\ a^+(1,S) + \sqrt{4/15}\ a^+(3,S)) - \sqrt{1/3}\ (a^+(1,L) + a^+(2,L))(s3-s0)$$

M(abc) is seen to be of the form $E(abc)(1+\sigma(abc)(s3-s0))$. Thus the observed rate divided by available phase space (called the reduced rate R(abc)) is approximately given by $|E(abc)|^2/n!$ where n is the number of pions in the same charge state. If the final state is pure I=1, $a^+(2,L)$ and $a^+(3,S)$ are set to zero with the immediate consequences:

$R(++-) = 4R(00+)$ (Dalitz's result)

$\sigma(00+) = -2\sigma(++-)$ (Weinberg's result)

Let us consider the K^0 decays. While the K^0 is the isospin eigenstate of interest, the state that decays into 3 pions is the CP-odd component K^0_2. The CP-even component K^0_1 cannot decay to 3 pions, or equivalently $\langle 3\pi|H'|K^0_1\rangle = 0$. Since $|K^0\rangle = \sqrt{1/2}\ (|K^0_1\rangle + |K^0_2\rangle)$ we have the result:

$\langle 3\pi|H'|K^0_2\rangle = \sqrt{2}\ \langle 3\pi|H'|K^0\rangle$.

Although the K^0_L is not a CP-odd eigenstate, the amount of CP-even admixture (ϵ) is of order 2 X 10^{-3} and is negligible for this consideration. Thus the above matrix elements for K^0_2 can be used for K^0_L as well. An inspection of the isospin states for K^0 shows that only the I=1,3 states are odd under CP. Thus with the obvious notation:

$$|f\rangle = a^0(1,S)|1,0(S)\rangle + a^0(1,L)|1,0(L)\rangle + a^0(3,S)|3,0(S)\rangle$$

Projecting out $|+-0\rangle$ and $|000\rangle$ in the final state gives:

$$M(+-0) = \left(\sqrt{1/15}\, a^0(1,S) + \sqrt{1/10}\, a^0(3,S)\right) + \sqrt{1/3}\, a^0(1,L)\,(s3-s0)$$

$$M(000) = -\sqrt{3/5}\, a^0(1,S) + \sqrt{2/5}\, a^0(3,S)$$

Immediately we see:

$$\sigma(000) = 0.$$

If we require pure I=1 in the final state we get:

$$2R(000) = 3R(+-0).$$

Since the possible transitions have ΔI = 1/2, 3/2, 5/2, or 7/2, the transition Hamiltonian can be written:

$$H' = H(1/2) + H(3/2) + H(5/2) + H(7/2)$$

where $H(n/2)$ transforms like an $I=n/2$ object under rotations in isospin space. The K^+ and K^0 matrix elements of H' are related through isospin invariance (Wigner-Eckart theorem - see for example reference 10). Thus for an irreducible tensor $T(JM)$ we have:

$$\langle j'm'|T(JM)|jm\rangle = C(jJj';mMm')\langle j'||T(J)||j\rangle$$

where we are computing the matrix element between states of definite angular momentum (isospin). The reduced matrix element on the right side does not depend on the 3RD component of isospin in the initial or final states. $C(jJj';mMm')$ is the Clebsch-Gordan coefficient to couple isospins j and J to get j' with the indicated projections m, M, and m'. We define reduced matrix elements:

$\lambda^{(n)} = \langle 1(S)||H(n/2)||1/2\rangle$ for n=1,3,

$\mu^{(n)} = \langle 1(L)||H(n/2)||1/2\rangle$ for n=1,3,

$\nu^{(n)} = \langle 2(L)||H(n/2)||1/2\rangle$ for n=3,5, and

$\eta^{(n)} = \langle 3(S)||H(n/2)||1/2\rangle$ for n=5,7,

in terms of which:

$$a^+(1,S) = \lambda^{(1)} - (1/2)\,\lambda^{(3)}$$
$$a^+(1,L) = \mu^{(1)} - (1/2)\,\mu^{(3)}$$
$$a^+(2,L) = \sqrt{3/4}\,\nu^{(3)} - \sqrt{1/3}\,\nu^{(5)}$$
$$a^+(3,S) = \sqrt{2/3}\,\eta^{(5)} - \sqrt{3/8}\,\eta^{(7)}$$

$$a^0(1,S) = \lambda^{(1)} + \lambda^{(3)}$$
$$a^0(1,L) = \mu^{(1)} + \mu^{(3)}$$
$$a^0(3,S) = \eta^{(5)} + \eta^{(7)}$$

A rigorous $\Delta I=1/2$ rule requires $\lambda^{(3)}=\mu^{(3)}=0$ with the predictions:

$$2R(00+) = R(+-0) \text{ and}$$

$$\sigma(00+) = \sigma(+-0).$$

CHAPTER II

THE APPARATUS

A K^0_L beam was run into the SLAC 2-meter streamer chamber. A system of scintillation counters and fast electronics was used to trigger the chamber on K^0_L decays Information necessary for the determination of the K^0_L time-of-flight was recorded on magnetic tape for each event. The chamber was located in a vertical 16 kilogauss magnetic field and was photographed in three views from above. Detailed descriptions of the chamber, the magnet, the beam, the electronics, and the optical system are given in the following sections of this chapter.

STREAMER CHAMBER

The streamer chamber is a particle detection device which renders visible (and hence photographable) the ionization left by a charged particle passing through its sensitive volume. It combines the 4 pi steradian solid angle acceptance of the bubble chamber with many of the advantages of a counter experiment. The chamber is triggerable which leads to a small number of pictures per event, allowing high statistics; and the pictures are generally devoid of irrelevant tracks. Also, multiple scattering is minimal since the sensitive volume contains gas (neon-helium mixture). The principles of streamer chamber operation have been reviewed in detail elsewhere[11], but will be discussed here both for completeness and as a prelude to a description of the special features of the K^0_L chamber.

1. Streamer Formation

If a high electric field is applied across a volume of gas containing a free electron, a discharge is initiated. This discharge spreads from the site of the electron along the direction of the electric field and will eventually go from electrode to electrode. However, if the voltage pulse is of very short duration, the spark is arrested and the result is a streamer. The streamer extends a few millimeters toward each electrode from the position of the original electron.

If photographed parallel to the field, it appears as a dot of light; looked at perpendicular to the field it is a streak. The exact details of the processes involved in the formation of a streamer are not at all well understood, but the basic explanation given below is thought to be essentially correct as far as it goes.

The growth of the streamer involves two phases. Initially the electron multiplies by ionizing gas molecules as it gains energy in the field. The resulting avalanche grows at a rate corresponding to the electron drift velocity in the gas. For 90% neon - 10% helium at a pressure of 760 torr and a field of 20 kv/cm (which is about 10 times the field required for static breakdown) the velocity is of the order of 10^7 cm/sec. The ion drift velocity is lower by about two orders of magnitude and so does not enter into the consideration. At a certain point the space charge of the avalanche transforms it into a streamer. The dominant process involved now is photo-ionization and the rate of longitudinal growth is at least ten times faster than the original avalanche growth. The photons form new avalanches, especially at the tips of the primary avalanche where the space charge intensifies the electric field. Thus the streamer grows longitudinally in both directions until the field is turned off. Although the streamer growth is symmetrical, the origin is displaced due to the fact that the space charge of the original avalanche drifts before the

avalanche is transformed into a streamer.

The electric field used for the formation of streamers is of the order of 15-20 kv/cm. To obtain this field over a 40 cm gap for a duration of 20 ns requires the use of special high voltage devices.

2. Marx Generator

The schematic of the Marx generator used to produce the high voltage pulse is shown in figure 1. All the components in the figure were located in a large tank of transformer oil. 47 capacitor banks, each containing 24 2000 pf barium titanate capacitors in parallel, were charged in parallel through carbon rod resistors to a voltage of about 22 kv. The output was obtained by discharging the capacitor banks in series through spark gaps so that their voltages added. A 23-gap manifold (switch tube) and a self-contained trigatron were used to accomplish this.

The 8' spark gap manifold contained 23 electrode pairs along a 6" diameter lucite tube which was filled with nitrogen gas at about 15 psi. A trigger disc sat midway between the electrodes of the first gap in the tube. The trigatron was triggered by a -15 kv pulse from a separate pulser outside the oil tank, and the resultant -2HV (±HV were the power supply voltages) output pulse appeared on the trigger disc, causing the first gap in the tube to break down. The series resistor R_S limited the current drawn through the trigatron, greatly prolonging its life.

Once the first gap of the tube had broken down, the rest of the gaps broke down sequentially by overvoltage. The design of the generator was such that the stray capacitances between the capacitor banks and ground, and from one bank to the other were much larger than the capacitances across the gaps, thereby ensuring that the overvoltage did in fact occur.

The DC supplies were modified to allow faster charging of the Marx generator. Rather than charging to 22 kv, the supplies were set to charge to 30 kv but cut off when 22 kv was reached. They were also modified so that there was a 5-10 ms delay after the Marx had fired before recharging began. This was to allow the switch tube to deionize so that it wouldn't break down again during the charging.

The problems of driving a large streamer chamber directly from the Marx generator are discussed in reference 11. The conclusion drawn is that an intermediate pulse shaping network is the best way to get the small risetime pulse necessary while allowing certain freedom in the design of the Marx.

3. Blumlein

A five electrode Blumlein line was used to provide the fast pulse. Figure 2 and the explanatory caption quoted below are taken directly from reference 11.

"The five-electrode Blumlein (a) is equivalent to two three-electrode Blumleins (b) each of which can be considered as a constant impedance line interrupted at the center by the load NZ. The first Blumlein pulse begins at time τ after the spark gap fires and continues until time 3τ where τ is the time required for a wave to travel from the spark gap to the end of the charged electrode. When the impedances of the Blumlein and load are properly matched (N=2), the amplitude of the first pulse is equal to the charging voltage, and all succeeding pulses are zero."

The spark gap was filled with sulphur hexafluoride gas at a pressure of 80-100 psi. Varying this pressure caused a variation in the breakdown voltage of the gap and hence in the voltage applied to the chamber. It is possible to design and build a Blumlein whose output voltage is very nearly equal to the voltage at which the spark gap breaks down[12]. However the Blumlein used in this experiment was only about 60% efficient with respect to voltage transmission due to a rather difficult and unfavorable geometrical configuration. Hence a Marx voltage in excess of a megavolt was required to apply 800 kv to the chamber. The pulse was monitored with a capacitive probe and had a width of 18 ns FWHM.

One point to note is that the chamber was subject to a rather long "prepulse" before the Blumlein gap broke down. The prepulse of opposite polarity to the main pulse was due to the charging of the Blumlein and caused the primary ionization to drift about 1 mm. This was only partially compensated by the displacement which occurred after the gap had broken down but before streamer formation had begun.

4. Chamber Construction

The streamer chamber used in this experiment was of the double gap design, thus providing twice the sensitive volume for a given voltage. This design also gives a symmetric configuration with the center electrode carrying the high voltage and the top and bottom electrodes being at ground potential. The gap size was 40 cm (for a total depth of 80 cm) as compared to 30 cm for the two previous chambers and the two later ones. This added size necessitated a higher Marx generator voltage for the same electric field, which was attained by using more capacitor banks and a higher voltage per stage.

The overall shape of the chamber was trapezoidal with a

length (along the beam) of 2 m. The upstream and downstream widths were 1.8 m and 1.1 m respectively. The walls were constructed of cast polyurethane foam slabs which were epoxied together and painted with dark green epoxy paint to minimize reflections. To cut down the amount of material in the beam the part of the front wall within the beam profile was recessed to present a 1" thick "window". The electrodes were very fine stainless steel mesh (.002" wire with .020" spacing) glued in an aluminum frame. The top and bottom of the chamber were .0015" mylar. Figure 3 gives an overall view of the streamer chamber and figure 4 shows the construction detail where the electrodes contacted the walls.

The trigger counters and particle identification plates were located inside the chamber (in the region of high electric field). To prevent electrical breakdown, they were enclosed in foam-walled boxes through which nitrogen gas was flowed. The aforementioned plates were intended primarily to identify electrons and so had to be made of high-Z material (like lead) to provide many radiation lengths per nuclear interaction length. However, due to their location in the chamber, they could not be conducting. Lead oxide (Pb^3O^4) and epoxy were mixed and cast into slabs that were about 1.7 radiation lengths thick. The density was 4.5 gm/cm^3.

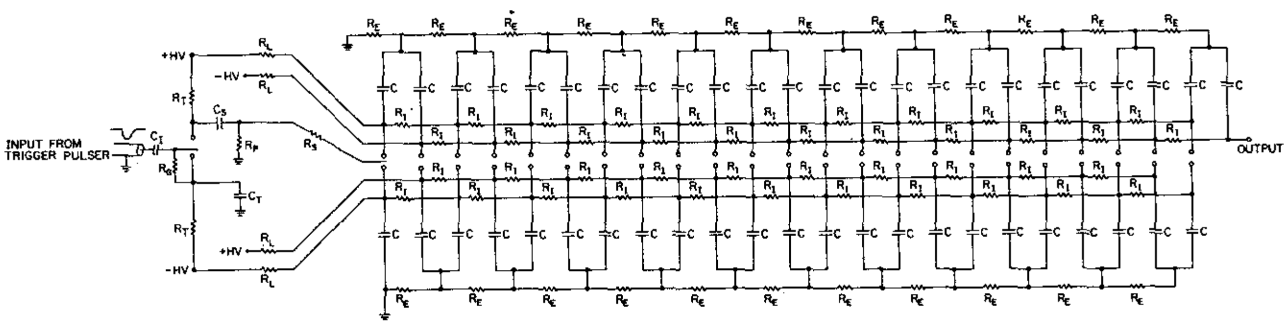

R_G GAP RESISTOR 20K, 6W
R_S SERIES RESISTOR 1K, 10W
R_T TRIGGER RESISTOR 3.6M, 40W
R_L LIMITING RESISTOR 50K, 200W
R_I INTERNAL RESISTOR 3K, 30W
R_E EXTERNAL RESISTOR 3K, 30W
R_P PARALLEL RESISTOR 50K, 10W

C_I INPUT CAPACITOR 900pF, 120 kV
C_S SERIES CAPACITOR 8000pF, 40kV
C_T TRIGGER CAPACITOR 8000pF, 40kV
C CAPACITY/STAGE 48,000pF, 40kV

Figure 1 - Marx generator schematic.

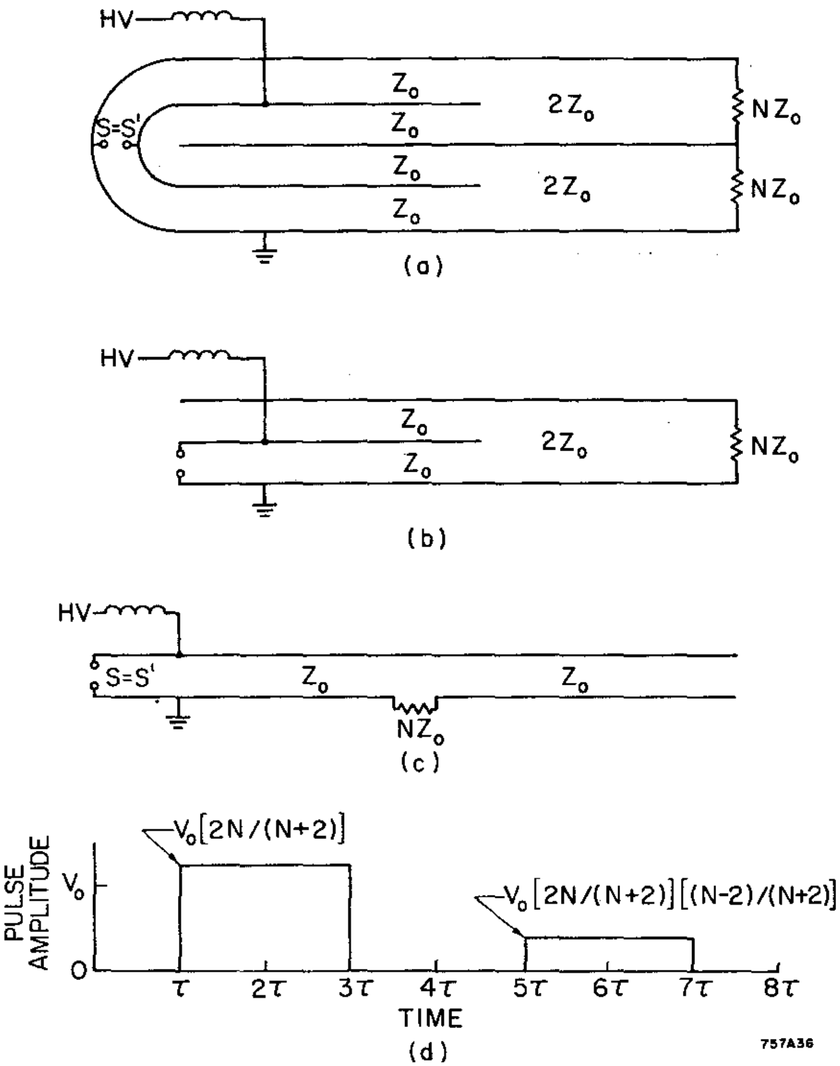

Figure 2 - Blumlein schematic and operation.

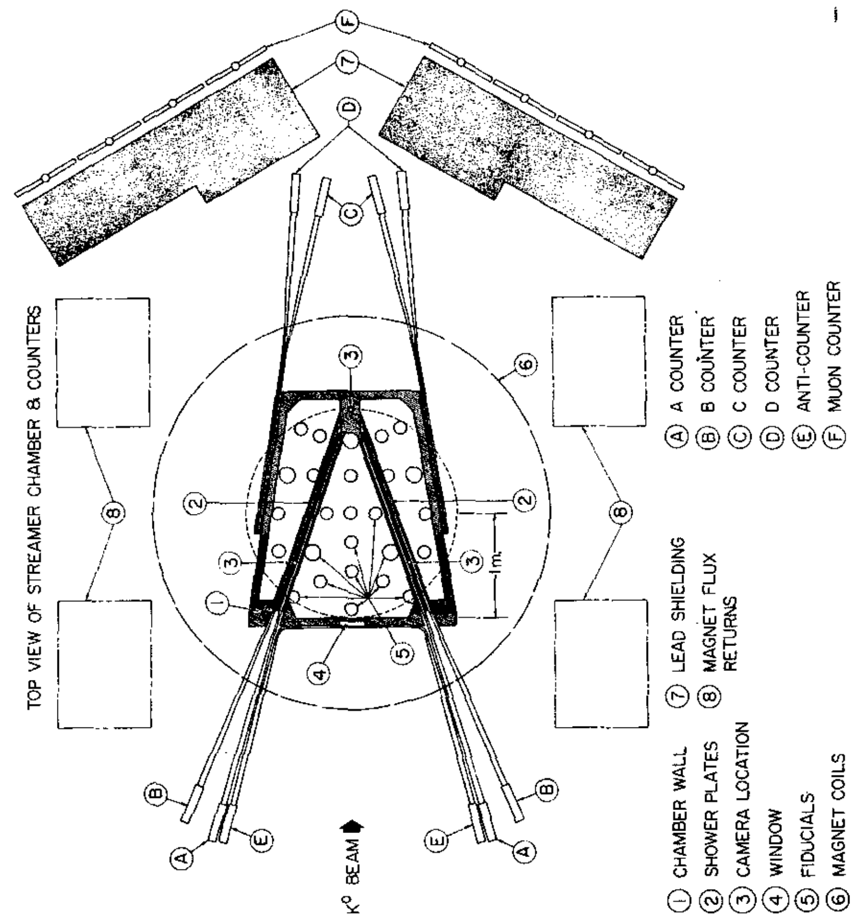

Figure 3 - Top view of streamer chamber and

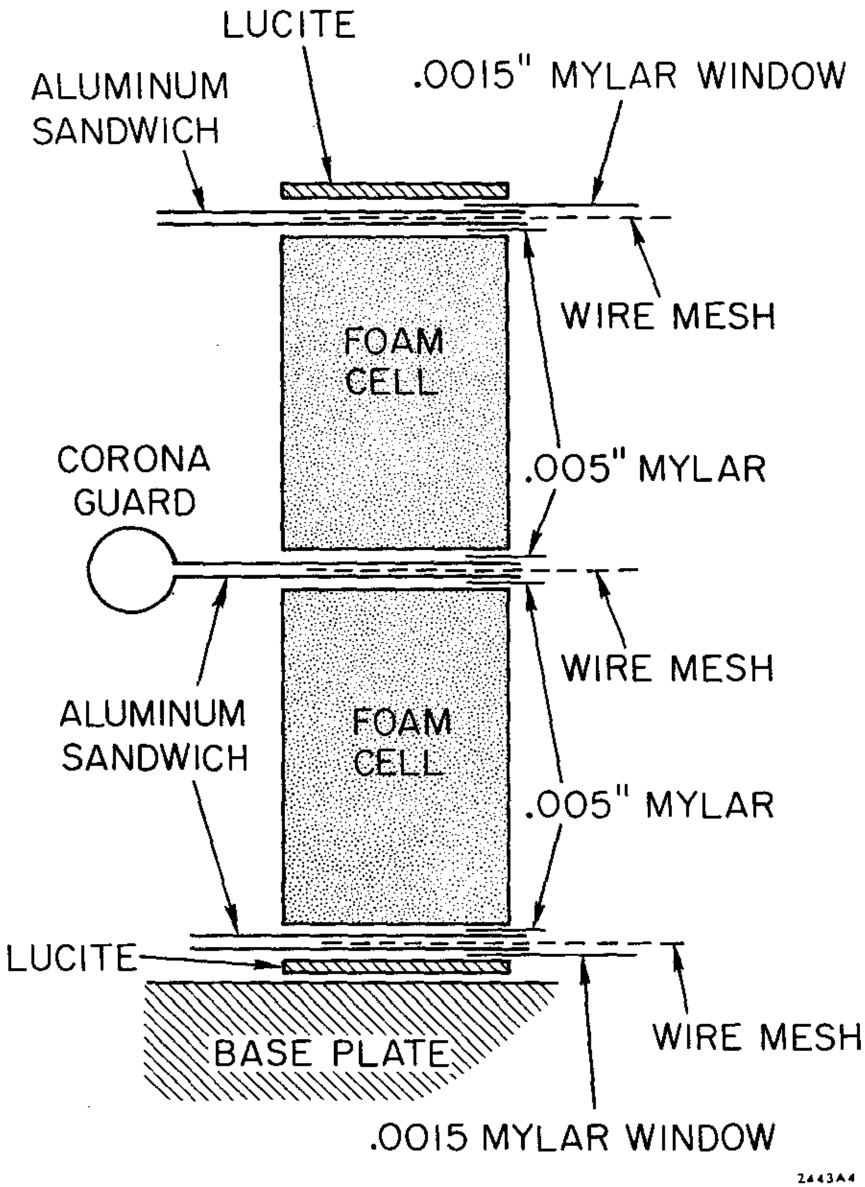

Figure 4 - Detail of streamer chamber wall.

1. Coordinate System

The streamer chamber was located between the polefaces of a 400 ton electromagnet, and the cartesian coordinate system used throughout the experiment was tied to this magnet. Marks on the front and back defined the x-axis and the beam was brought in within a few milliradians of this line. The z-axis was taken as the axis of cylindrical symmetry of the coils (vertical - pointing up) and the y-axis so as to form a right-handed coordinate system. The origin was 1 m upstream and 50 cm above the center of the bottom poleface.

The direction of a given vector was defined by the angles λ (latitude) and ϕ (azimuth). λ was the angle between the vector and the x-y plane; ϕ was the angle between the vector which had been projected onto the x-y plane and the x-axis. In terms of these angles, the cartesian components of a unit vector (ux,uy,uz) are:

$ux = \cos\lambda\cos\phi$

$uy = \cos\lambda\sin\phi$

$uz = \sin\lambda$

2. Magnetic Field Determination

The magnet was powered by a 5.8 megawatt power supply and provided a field of about 16 kilogauss over a cylindrical region 2 m in diameter and 1 m in height. The field was continuously monitored by three Hall probes mounted on the bottom poleface and a shunt reading of the magnet current. A nuclear magnetic resonance probe could be lowered from above into a region of uniform magnetic field to give an absolute calibration. The upper poleface was open to allow photography along the magnetic field direction. This resulted in field inhomogeneities of 15-20% in the z component and a non-negligible radial component (up to 5 kilogauss), necessitating a precise field map.

The three cartesian components of the field were measured in eight horizontal planes. Measurements were taken on a grid the spacing of which was .025 m in x and .102 m in y. The planes were at a .102 m separation in z. Three mutually orthogonal coils mounted on a carriage were moved from point to point (of the aforementioned grid) and the flux changes were recorded. Due to the large fringe field of the magnet and the limited length of the tracks on which the carriage ran, it was impossible to move the coils to a field-free region. Hence the flux changes were taken relative to a central point whose field was measured by nuclear magnetic resonance.

In order to make these magnetic field measurements available to the analysis programs, it was necessary to express them

in analytic form. The cylindrical symmetry of the magnet suggested the choice of variables, namely z and r where $r=\sqrt{(x-1)^2+y^2}$ (recall that the center of the magnet was at x=1m). Three regions of r were considered out to 2 meters and the field was set to zero beyond that. The radial component was expressed as a polynomial and the vertical component as an inverse polynomial (to allow the rapid falloff observed in the measurements). There were 100 parameters in all, which were adjusted by a least squares fitting program to give the best agreement between the analytic form and the measurements. The agreement was typically good to about 30 gauss.

BEAM

1. Physical Layout

The K_L^0 beam was produced by hitting a 70 cm beryllium target with an electron beam whose energy varied between 14 and 16 GeV during the course of the experiment. The electron beam was deflected by .8° to the right before hitting the target, and the particles coming off at 5.8° to the left (5° from the original undeflected beam) were passed through a 12" lead filter to remove gamma rays. There were four 10' steel collimators (hereafter referred to as 13C1, 13C2, 13C3, and 13C4). There were sweeping magnets after 13C1 and 13C3 to remove charged particles. 13C3 and 13C4 each had a horizontal septum to remove particles from the median plane so that they did not hit the central electrode of the streamer chamber. 13C4 was oversize and served only to remove background and halo. The beam was run in air up to 13C2 and in helium from there on to cut down nuclear scattering of the K_L^0's. As is seen in figure 5 the chamber was approximately 100 meters from the target.

2. Chopped Beam

In SLAC's normal operation, beam is delivered in very short bursts (about .01 ns) at 1/3 ns intervals for the duration of the beam pulse which lasts 1.6 μs. This natural

structure arises as follows. The sixth harmonic of a very accurate and stable 476 mc oscillator is used to modulate the klystrons. The electrons are injected into the machine over a narrow phase range (about 5°) of this 2856 mc at the proper time in the cycle to get acceleration (see figure 6). Thus the shortness of the spikes arises from the narrowness of the phase (necessary for good energy resolution) and the 1/3 ns (or more precisely 1/2.856 ns) comes from the frequency applied to the klystrons.

For certain applications, the accelerator is run in the "chopped beam" mode, whereby the time between spikes is increased from 1/3 ns to 50 ns or more (with the same 1.6 μs total pulse length). This is accomplished by applying an electromagnetic field transverse to the beam at a frequency which is an integral fraction of the basic 476 mc. The only spikes that are transmitted are the ones that occur at the zero crossing of the deflection field. By varying the frequency (or frequencies) applied to the deflection plates, one is able to get different spike intervals (called chops). A typical chop used in this experiment was 150 ns. Figure 6 shows the time structure of the beam in both the normal and chopped modes.

The reason for using the chopped beam mode was to allow precise timing so that the time-of-flight (and hence the momentum) of the K_L^0 could be determined. Also cf importance was the fact that the electronics could be kept sensitive over a time interval that tended to exclude photon and slow neutron interactions from the trigger. Had the chop been much shorter than 150 ns, slow neutron interactions from an earlier spike would have occurred during the time slot that the electronics was sensitive; had it been much longer, the overall trigger rate would have been lower. Although parts of the film were taken at 100 ns and 200 ns chop, the bulk was taken with 150 ns.

The timing of all the electronics was based on a direct signal generated at the target when the K_L^o was produced. The end of a coaxial cable had its central conductor stripped bare and placed in the beam line right at the target. When the beam hit this detector, secondary electron emission caused a positive pulse which was sent to the experimental area. Special "air dielectric" cable was used to minimize the dispersion of the extremely narrow pulse.

THIS PAGE LEFT BLANK.

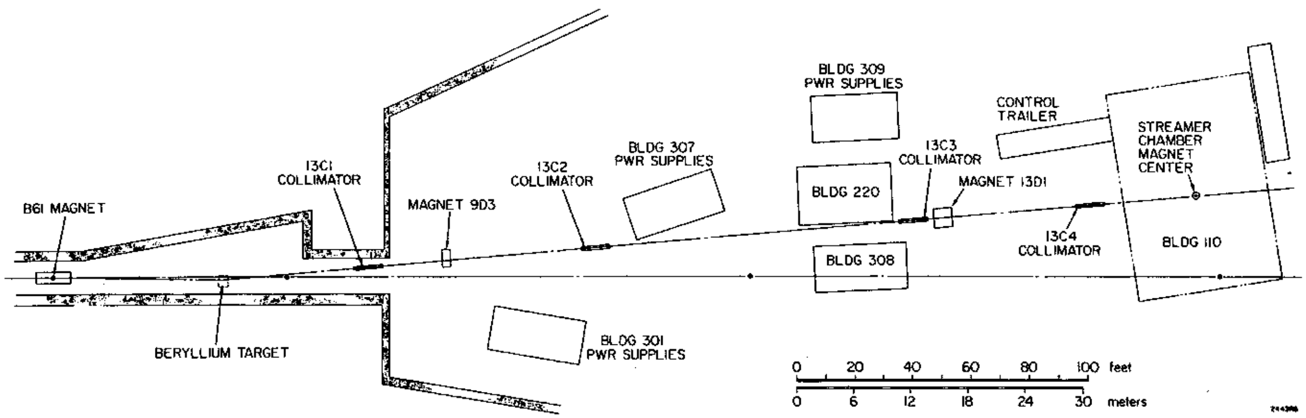

Figure 5 - Beam layout.

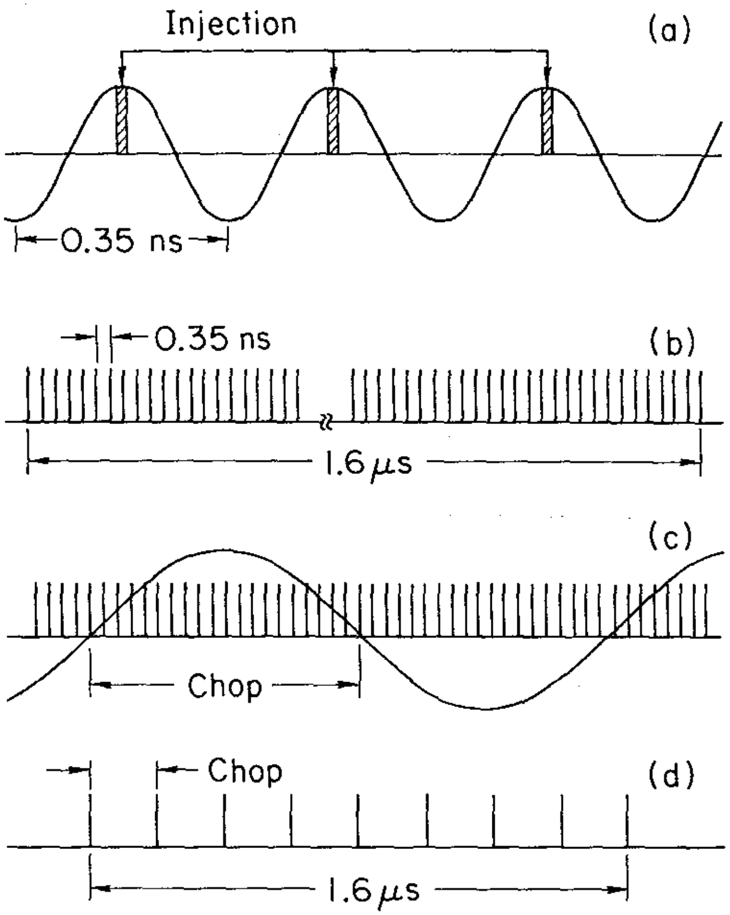

(a) Origin of Normal rf Structure
(b) Normal Beam Pulse
(c) Application of Deflection Field
(d) Chopped Beam Pulse

7443812

Figure 6 - Radiofrequency structure of beam pulse.

ELECTRONICS - COUNTER LOGIC

In order to trigger the chamber on K^0_L's, a setup of scintillation counters and fast logic was used. The counter electronics (discriminators, coincidence circuits, analog to digital converters (ADC's), etc.) were located in an RF-shielded room right next to the magnet so that the trigger logic could be done with a minimum of delay. The on-line computer and the other electronics which came into play when an event occurred were located in the control trailer 50' away. This represented a transit time of about 200 ns, since the cables went from the shielded room to the trailer via patch panels.

1. The Counters

Figure 3 is a top view showing the location of the counters in and around the streamer chamber. Each counter in the diagram actually represents two counters, one above the plane of the streamer chamber center electrode and one below it. The phototube of each counter was enclosed in a large cylindrical steel magnetic shield. Inside the chamber were eight counters which were used in the trigger and provided timing information. These "A" and "B" counters were 4' long and 40 cm high. Immediately around the chamber were four "C" and four "D" counters (each 6' long and 40 cm high), and four "chamber" anti counters. The C and D counters provided additional timing information while the anti counters were used in the trigger. The numbering of the A, B, C, D, and anti counters was such that facing along the beam, #1 was upper left, #2 was lower left, #3 was upper right, and #4 was lower right. Not shown in the diagram are ten anti counters (a right and left wall of five each) about 20' upstream of the chamber.

The A, B, C, D, and chamber anti counters were made of 1/2" thick Pilot M scintillator plastic. The muon and wall anti counters were made of NE110 which had a longer decay time (2 ns as opposed to 1.3 ns). Thus while the Pilot M light output was no greater than that of the NE110, the output pulse was better resolved in time and gave better photocathode statistics.

The phototubes of all the counters except the A's and B's were Amperex 56 AVP's. The RCA C31000D phototubes used on the A and B counters were characterized by a somewhat higher photocathode efficiency (about twice that of the 56 AVP's) and a much higher gain at the first dynode. The effect of this higher gain (about 80 compared to about 2) was to reduce the statistical fluctuations in pulse height due to small numbers of electrons at early stages in the multiplication.

One of the outputs of each A, B, C, D, and muon counter

discriminator was fed into an EG&G DG102 gated latch. The thirty two DG102's thus provided a record of which counters fired in each event. The gate for the DG102's was provided by a master trigger which is described below. Both the raw phototube pulse and the discriminator output of the A, B, C, and D counters were sent to ADC's for the time of flight determination.

2. The Trigger

As can be seen from figure 7, the basic trigger consisted of an A-B coincidence (thereby requiring the presence of a charged particle inside the chamber) in anticoincidence with the anti counters in front (to ensure that the triggering particle originated inside the chamber). The details are outlined below.

The A and B phototube outputs were each put into a Lecroy 611 Dual Discriminator, and one of the outputs (there were two pairs on each discriminator) was clipped to 8 ns. This was accomplished by attaching a 4 ns cable, shorted at the end, to the other output of the pair, thus providing a very stable pulse length. Each quadrant's A and B were put into coincidence and the output of each "and" was clipped to 8 ns. The logical "or" of the four A-B coincidences formed M_o, the main ingredient of the trigger.

The phototube outputs of the five anti counters in each of the upstream walls were tied together at the phototubes thereby making each wall effectively one large counter. The four chamber anti counters and the two wall anti outputs were each connected to an EG&G TR204 discriminator. The TR204 had two features that were very important for its use in the veto. First of all it was a DC pass discriminator, which meant that the output remained after the fixed pulse length that had been set (30 ns in this case) if the input from the phototube was still above threshold. Secondly the discriminator was deadtimeless. A discriminator without this feature would have been insensitive to a second input pulse if there had still been output from a first pulse. The TR204 on the other hand, extended the output to last 30 ns (in this case) from the latest input, and more if the DC pass feature came into play. The logical "or" of the antis was thus on for at least 30 ns from the latest input. The compliment of this was put in coincidence with M_c to form M_c' which was clipped to 30 ns.

The timing pulse (described in the section on the beam) was inverted (being positive originally) and sent through a discriminator. The output width was set to 2 ns, and this signal, called T, was put in coincidence with M_c' to form MT, the master trigger. The relative cable lengths were set so that the earliest M_c' finished just after T ended when muons (nearly v=c) were run into the chamber. Thus, except

for the very slowest of particles, which were later eliminated from the sample, the timing of MT was determined by T. This was important for the timing considerations which follow.

3. Time and Amplitude ADC's

In order to measure the time of flight of the K_L^o, it was necessary to have information regarding the timing of the A, B, C, and D counter pulses relative to the timing pulse. Since the discriminator output was used to establish the counter timing, a pulse which took a long time to rise to threshold due to a small amplitude would give a time which was too late. Hence it was also important to know the amplitude of the pulse, to allow a timing correction to be made. The details of extracting an actual K_L^o momentum from the ADC information are described in another chapter. Below is a description of how the ADC information was obtained.

The ADC's which were used gave an output proportional to the time integral of the input as long as a gate pulse was present. There were two ADC's per counter (time and amplitude). There were also ADC's for the purpose of monitoring the Marx and Blumlein voltages and the time and amplitude of T. (If T's time wasn't constant with respect to the trigger, it meant that the timing of MT had not been set by T.)

Each time ADC got a 38 ns gate from MT. Since the timing of MT was determined by T, this was in essence a T gate for timing considerations. The unclipped output of the counter discriminator was set to have a width of 35 ns and was put into the ADC. The later this pulse was (relative to MT), the smaller the overlap measured by the ADC. This is shown in figure 8.

Each amplitude ADC got a 60 ns gate from MT and the raw phototube pulse was fed into the ADC. The gate had to be long enough to contain the rather long pulse over the entire range of times. Since the ADC measured the time integral of the pulse, the "amplitude" reading could be misleading. Several small amplitude pulses within the gate interval would simulate a large amplitude by giving a large reading.

Calibration of the time ADC's was done eleven times over the course of the experiment during periods when data was not being taken. The purpose was to allow the conversion of the ADC reading to nanoseconds. The output of a mercury switch pulser was fanned out to the T discriminator and to the light diodes which were epoxied to the light pipes of the A, B, C, and D counters. The length of the cable to the T discriminator was varied by inserting cables whose length in nanoseconds had been accurately measured. Typically, 1000 of these simulated events for each time setting were read into the computer at rates of the order of 10/second.

Subsequent analysis of the computer tape allowed the extraction of calibration curves.

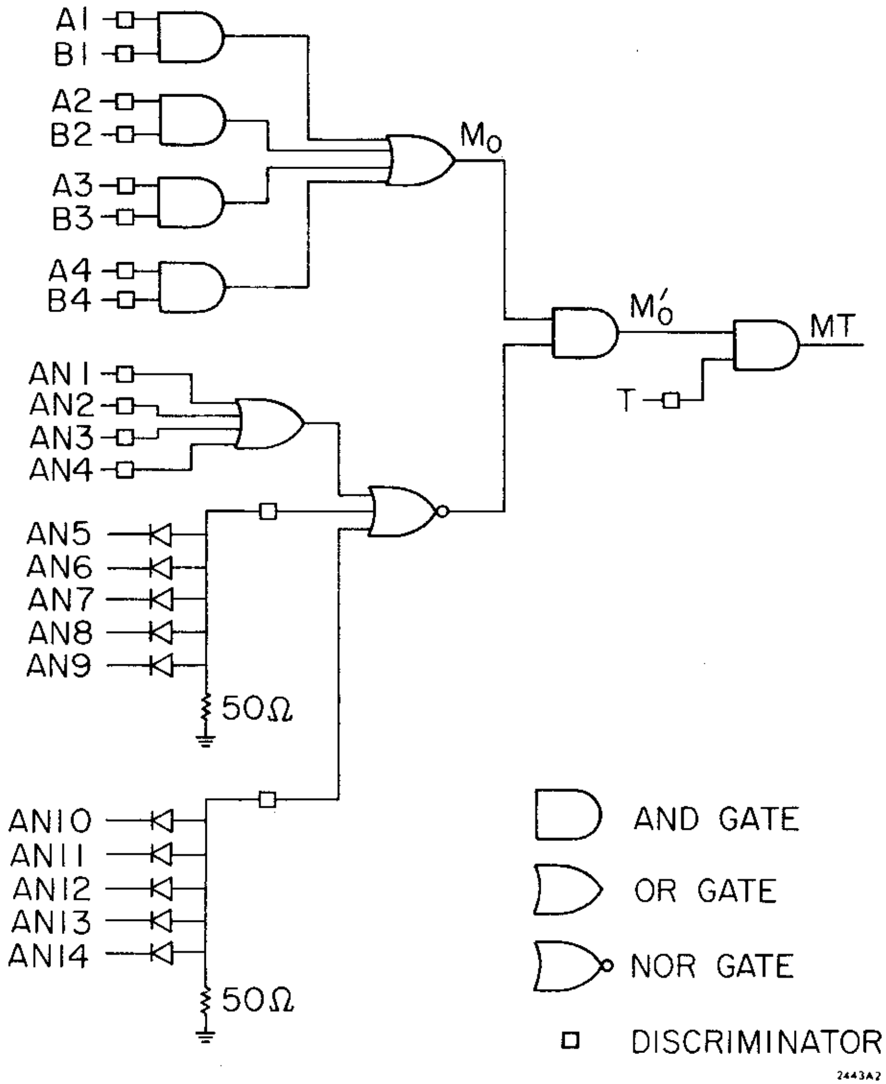

Figure 7 - Trigger logic.

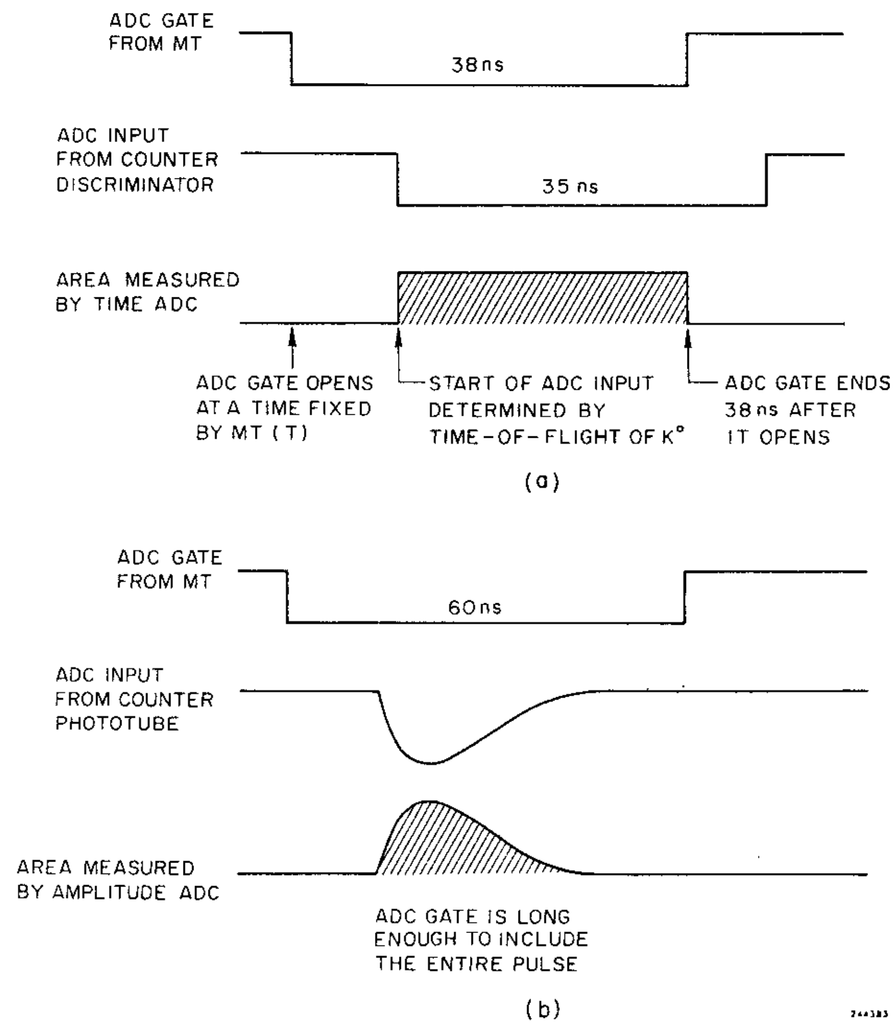

Figure 8 - Time and amplitude ADC gates.

ELECTRONICS - EVENT SEQUENCE

1. Machine Gate

A "machine gate" pulse was sent from the accelerator control room 2.5 μs before the start of the beam pulse. This pulse was used directly to reset the DG102's. It was also delayed for 2 μs and a 2.5 μs pulse was generated to activate the electronics, thus keeping them sensitive over an interval completely spanning the beam pulse. It is this delayed pulse which will be referred to hereafter as the machine gate. When an event occurred, it was necessary to kill the machine gate in order to prevent another trigger before the event had been completely processed. The term "dead time" refers to the time during which the electronics were disabled for this purpose. In particular, a dead time of approximately 400 ms was necessary to allow enough time for the Marx generator to charge up. Since the module generating the gate was in the control trailer (physically removed from the trigger logic), the electronics would have still been sensitive during the next beam spike. To avoid this, MT was used to inhibit the T discriminator, thus making it impossible to get another trigger before the electronics had been disabled.

2. Trigger Pulse

The occurrence of an event was signalled by an MT pulse as has been described in a previous section. This pulse was fanned out to several destinations to accomplish the following:

a) suppress the machine gate for 5 μs until the electronics in the control trailer could suppress it for a longer period (typically 400 ms),

b) trigger the Marx generator,

c) reset the ADC scalers and gate the ADC's,

d) gate the DG102's,

e) interrupt the computer in preparation for reading in the data, and

f) pulse "Guisseppe", a digital time sequence generator, to initiate the series of tasks described below.

3. Guisseppe

Guisseppe[13] was essentially ten gate generators built into a single unit. Each gate could be set to begin and end at any specified times (within design limits) of the initial pulse. The setting was done by inserting pegs into holes in the pegboard-like front face. Both logic (-0.7 volts) and gate (+10 volts) levels were available.

Starting immediately from the initial pulse, pulses of varying widths were sent to do the following:

a) flash the fiducials,
b) flash the data boxes on the cameras,
c) kill the machine gate for about 400 ms, and
d) suppress the beam if we were in beam-sharing mode to let other experiments make use of the beam pulses during our dead time.

At later times in the sequence pulses were sent to:

e) advance the cameras,
f) advance the frame number, and
g) have the digital voltmeter (DVM) step through its sequence of reading one phototube voltage per event.

4. On-line Computer

A PDP-9 computer manufactured by Digital Equipment Corporation was used to record the counter data for each event on magnetic tape. In addition to the DG102 and ADC information, the tape record included the roll, frame, date, phototube voltages, and the shunt and Hall probe readings for the streamer chamber magnet. As well as recording event data, the computer was used to monitor what was being accumulated. Histograms of the ADC readings were built up in core and displayed on a scope screen for observation. If certain quantities (chamber voltage, magnetic field, counter voltages) ever got outside specified ranges, warnings were

printed on the teletype so that the appropriate corrective action could be taken.

The data was sent to the computer in the form of 16-bit words on a 16-line data bus. The ADC's were 8 bits each, so the time and amplitude ADC for each counter were linked to form one word. The thirty two DG102's formed two words, and each other device (DVM's, roll number, etc.) had four 4-bit BCD digits and thus formed a single word. In all there were 28 words, which were put on the data bus in sequence. The method of getting the ADC information onto the bus was different from that for the other data.

Each non-ADC device's 16 bits were fed into a multiplexer. One line on the multiplexer per device could be strobed to put that device's output onto the data bus. (The multiplexer had the function of a 16 pole-multiple throw switch.) The ADC's on the other hand, did not require an external multiplexer. In response to a read gate pulse a given ADC would put its 8 bits on the line. (Thus each ADC in effect had its own 8 pole-single throw switch.)

The sequential reading of the data was controlled by three strobe generators (called "Arturo"). The Arturo's were set up serially so that in response to computer pulses, each word would be read into the computer. The strobe for the ADC's went to the appropriate ADC read gates; the other strobes went to the multiplexer. A schematic of this is shown in figure 9.

The reading was done on the data channel which was much faster than reading under program control through the computer's accumulator. The program would issue a command to read, and would be interrupted when all the data had been read into core.

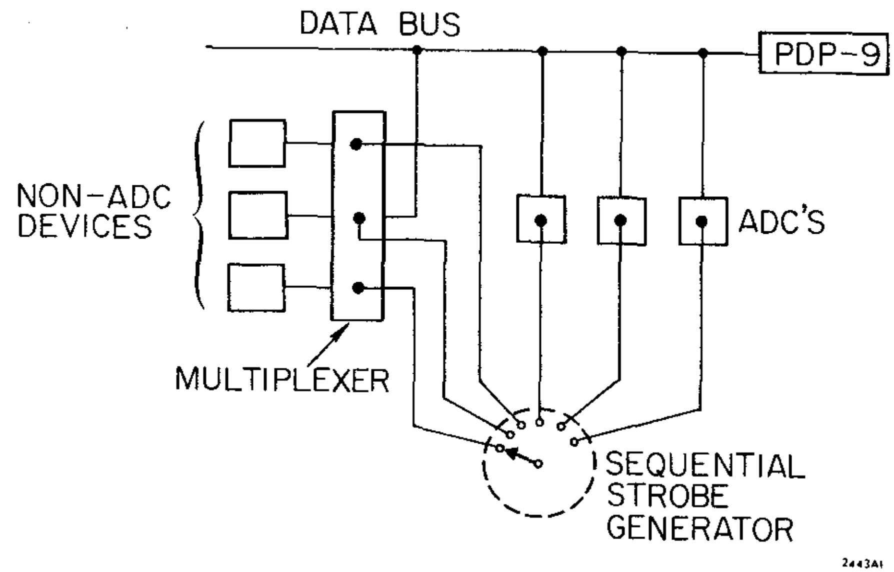

Figure 9 - Data bus schematic.

OPTICAL SYSTEM

1. Fiducials

Three cameras located about 4 m above the streamer chamber were used to photograph the events in 18° stereo. In order to relate the photographs to real space, it was necessary to include some reference marks (fiducials) in the pictures. Each fiducial was constructed from an electroluminescent panel which was masked to allow only a fine cross to shine through (2.5 mm lines). Twenty six fiducials were mounted on a marble plate which was attached rigidly to the magnet poleface below the chamber, and five were mounted on beams just above the chamber. Five of the lower fiducials were larger than the rest and were used in the event measurements. All thirty one were used in the optical constants' determination.

2. Cameras and Film

Model 207 aerographic cameras manufactured by Giannini Scientific Corporation were used. They were extensively modified and upgraded to provide a high level of reliability and accuracy. The film transport system was improved by the introduction of vacuum loops so that the film was under a constant tension of 8 ounces. This allowed the use of 1200' rolls of film, whereas previously 300' had been an upper

limit for reliable operation. Vacuum platens whose surfaces had been optically lapped were substituted for the conventional pressure platens and all critical surfaces were remachined and polished. The cameras were equipped with data boxes so that important information (roll, frame number, magnet shunt reading, etc.) appeared in the picture. The cameras were notable in being able to run in a random pulse mode at up to 15 shots per second, i.e. the film could be advanced within 1/15 second of receiving an "advance" voltage pulse. There were no shutters as the streamer chamber was completely dark except when it was being pulsed.

The lenses were Summilux 50mm f/1.4 made by E. Leitz. The aperture used during most of the data taking was f/2.4 which gave a reasonable compromise between good depth of field and adequate exposure. The distortion of off-axis rays was measured on an optical bench and was found to be well described by the formula:

$$d = c.\tan^5\theta$$

where:

d is the distortion on film radially from the optic axis,

c is the distortion parameter, and

θ is the angle between the image ray and the optic axis.

The actual distortion parameter used in all computations was c/f^5 where f was the focal distance of the lens.

A special film was developed for SLAC by Eastman Kodak for use in photographing the streamer chamber. SO 265 (Special Order 265 - formerly SO 340) is a very fast panchromatic film with an extended red sensitivity (Aerial Exposure Index of 250 which is roughly comparable to an ASA of 2000-3000). This high speed coupled with a resolving power of 71 lines/mm made the film eminently suitable for aerial photography as well. Kodak Tri-X Aerographic Film 2403 is identical to SO 265 except that it has a fast-drying base whereas SO 265 does not[14]. The film was typically processed to a gamma of 1.6.

CHAPTER III

DATA REDUCTION

The ultimate purpose of the data analysis was to obtain an unbiased, pure sample of 3 pi decays from which to extract physical quantities. Before this could be done, the film was scanned and measured, optical constants were computed, and the track measurements were fitted to obtain the particle momenta. A general description of the kinematics of K^0_L decays and a summary of certain methods of analysis used in the above data reduction are given below. The data reduction is then described in detail.

KINEMATICS OF K^0_L DECAYS

In this section we consider the kinematic features of the data without the kinematic fitting. The procedures and results of the kinematic fit are discussed in a later chapter.

1. General Features

The three decay modes considered here are:

$K^0_L \longrightarrow \pi^+\pi^-\pi^0$ (K3pi or 3 pi)

$K^0_L \longrightarrow \pi^\pm\mu^\mp\nu$ (Kmu3)

$K^0_L \longrightarrow \pi^\pm e^\mp\nu$ (Ke3)

The unknowns in the problem are the three momentum components of the unmeasured neutral particle and the magnitude of the K^0_L momentum. (The time-of-flight information is not considered in this part of the discussion). The four equations of energy and momentum conservation thus lead to the solution for the four missing quantities. It is clear that once the K^0_L momentum is known, the missing neutral's momentum is easily found, so let us consider the solution for the K^0_L momentum. The solution is most easily obtained by writing the 4-momentum equation:

$$P0 - (p1+p2) = p3$$

where:

P0 is the K^0_L 4-momentum, and

p1,p2,p3 are the 4-momenta of the positive,negative and neutral decay particles respectively.

Forming the Lorentz square of both sides (thereby eliminating the neutral particle's momentum) and computing in the laboratory frame leads to:

$$|\vec{P0}| = \frac{B[p1(par)+p2(par)] \pm (E1+E2)\sqrt{B^2-M0^2(M12^2+Pt^2)}}{(M12^2+Pt^2)}$$

where:

$B=(M0^2+M12^2-m3^2)/2$

M0 is the K^0_L mass,

M12 is the invariant mass of the two charged particles,

m3 is the mass of the neutral particle,

p1(par),p2(par) are the 3-momentum projections of the charged particles parallel to the K^0_L momentum,

E1 and E2 are the energies of the charged particles, and

Pt is the total visible transverse momentum.

Writing the 4-momentum equation as

$$P0 - p3 = (p1+p2) ,$$

forming the Lorentz square of both sides, and evaluating the left side in the c.m. where the K^0_L 3-momentum vanishes gives:

$E3 = (M0^2 + m3^2 - M12^2)/(2M0)$

$T3 = [(M0-m3)^2 - M12^2]/(2M0)$ with the obvious maximum

$T3max = [(M0-m3)^2 - (m1+m2)^2]/(2M0)$, and

$q3^2=T3(T3+2m3)$

where:

E3 is the c.m. energy of the neutral particle,

T3 is the c.m. kinetic energy of the neutral particle, and

q3 is the magnitude of the neutral's c.m. 3-momentum.

The origin of the quadratic ambiguity in $|\overrightarrow{P0}|$ is more easily seen now. The neutral's transverse momentum in the c.m. is known (being given by -Pt), and the square of the neutral's 3-momentum in the c.m. is known from the kinetic energy. Hence the magnitude (but not the sign) of the neutral's c.m. longitudinal 3-momentum can be found, since

$q3(par)^2 = q3^2 - Pt^2$.

Thus the quadratic ambiguity is merely the uncertainty as to whether the neutral particle is going forward or backward in the c.m.

Due to the quadratic nature of the solution, it is possible that an event will have an imaginary solution for the K^0_L momentum, i.e. the event can be unphysical for the given decay hypothesis. This fact is exploited to allow a partial identification of the decay mode. Due to the masses of the particles involved, a true 3 pi decay will also have solutions for the semi-leptonic modes. The converse is not

so however. Most (about 95%) of the true semi-leptonic decays do not give a solution if they are assumed to be 3 pi decays.

While the discriminant (assuming a 3 pi decay) contains the required kinematic information, it is customary to use a different quantity when talking about identification of the decay mode. $(P0')^2$ is defined as the square of the K^0_L momentum in the frame where the visible momentum is all transverse. It has the same sign as the discriminant for the 3 pi hypothesis, as can be seen from the first of the two equivalent expressions.

$$(P0')^2 = \frac{(M0^2+M12^2-m3^2)^2 - 4M0^2(M12^2+Pt^2)}{4(M12^2+Pt^2)}$$

$$(P0')^2 = \frac{(M0^2+m3^2-M12^2)^2 - 4M0^2(m3^2+Pt^2)}{4(M12^2+Pt^2)}$$

where the quantities on the right now refer specifically to the 3 pi hypothesis (e.g. m3 is the π^0 mass). The $(P0')^2$ distribution for the data (all three modes) is shown in figure 12.

2. Dalitz Plot and the π^0 Kinetic Energy

In studying the 3 pi decay of the K^0_L it is customary to plot the center-of-mass kinetic energies of the pions on a Dalitz plot[15]. An event is represented by a point inside an equilateral triangle of altitude Q $(Q=M0-m1-m2-m3)$. The kinetic energies of the three pions are given by the distance of the point to the respective sides, thereby ensuring energy conservation. This is equivalent to plotting y vs x where the Dalitz variables are given by:

$$x = (T2-T1)/\sqrt{3}$$

$$y = T3 - Q/3$$

The phase space element is given by the area element on the plot[16], and the points are constrained by 3-momentum conservation to lie inside a nearly circular boundary. Alternately, one plots the kinetic energy of the π^+ (T1) against that of the π^- (T2). The phase space element is now simply the area element in T1-T2 space, and the contours of constant T3 are straight lines at 45° to the axes.

The phase space for decays at a fixed T3 is given (aside from normalization) by the separation of the twc points where the constant T3 line intersects the Dalitz plot boundary.

$$\text{phase space} = \sqrt{q3^2(M12^2-4m1^2)/M12^2}$$

which depends on T3 only, since $q3^2=T3(T3+2m3)$ and $M12^2=(M0-m3)^2-2(M0)(T3)$.

3. Measurement Errors and the "0C" Fit

Since the solution for the K^0_L momentum involves a quadratic equation, it is possible that random measurement errors will

make some 3 pi decays unphysical (negative discriminant or equivalently, negative $(P0')^2$). This effect is particularly significant since the $(P0')^2$ distribution of ideal events is strongly peaked at 0 (see figure 10).

The formal way that this difficulty is handled is to constrain the discriminant to vanish and do a fit. Events that fail this fit can be tentatively identified as being semileptonic decays or some other contamination. The fit is loosely (and strictly speaking incorrectly) referred to as a 0C (zero constraint) fit in the sense that the constraint is not introduced a priori (as energy-momentum conservation is).

4. Timing Information and the 1C Fit

With the addition of the time-of-flight measurement, the problem becomes a true 1C (one constraint) fit, since there are now 4 equations (energy-momentum conservaticn) and only 3 unknowns (the 3-momentum of the neutral decay product). Basically the events that fail this fit fall into two classes. Either the momenta are such that the event is unphysical, or the timing information disagrees with the other kinematic results. The former would fail the 0C fit; the latter would pass. This distinction is sometimes helpful with certain classes of contamination. Before discussing the detailed procedures and results cf the 1C fit, it is helpful to consider some of the alternatives.

The time-of-flight measurement of the K_L^0 momentum can be compared with the values calculated from the charged particle momenta, and the best solution picked. At this point it must be decided whether the mode identification has been made uniquely and whether the quadratic ambiguity has been resolved. While such a procedure is capable of identifying some events, several problems remain which are difficult or impossible to resolve without resorting to a kinematic fit.

Due to random measurement errors, the solutions have errors associated with them. The timing information has its own error, so any comparison method must take into account all the errors and have some prescription for evaluating the uniqueness of the identification. Once an identification has been made, the timing information is normally not considered any more, so the data has clearly not been exploited to the maximum extent. Furthermore, an attempt to incorporate the timing information into the K_L^0 momentum value without doing a fit is almost certain to lead to values of momenta that violate 4-momentum conservation.

Another method which can be used to pick 3 pi events is to select on the basis of the mass squared of the missing neutral assuming both charged particles to be pions. The

missing mass squared is given by:

$$MM^2 = (P0-p1-p2)^2$$

where:

P0 is the K_L^0 4-momentum from timing,

p1 and p2 are the assumed pion 4-momenta from geometry, and

MM is the missing mass.

The semileptonic modes give values of MM^2 over a broad range including negative values, while the 3 pi decays show a distribution sharply peaked at the π^0 mass. See figure 11 for the observed distribution of MM^2. This is a useful way to display the data, but is generally unsuitable as the sole selection method. It is difficult to estimate the loss that occurs when a cut on the missing mass is made, and it is impossible to identify semileptonic contamination. As in the previous method the measured values have not been adjusted to take all the information into account and to conserve 4-momentum. Moreover the quadratic ambiguity remains unresolved.

The 1C kinematic fitting procedure suffers from none of the above difficulties. Also, it allows a determination of how well the data approximates the ideal statistical behavior assumed. A detailed discussion is deferred until a later chapter.

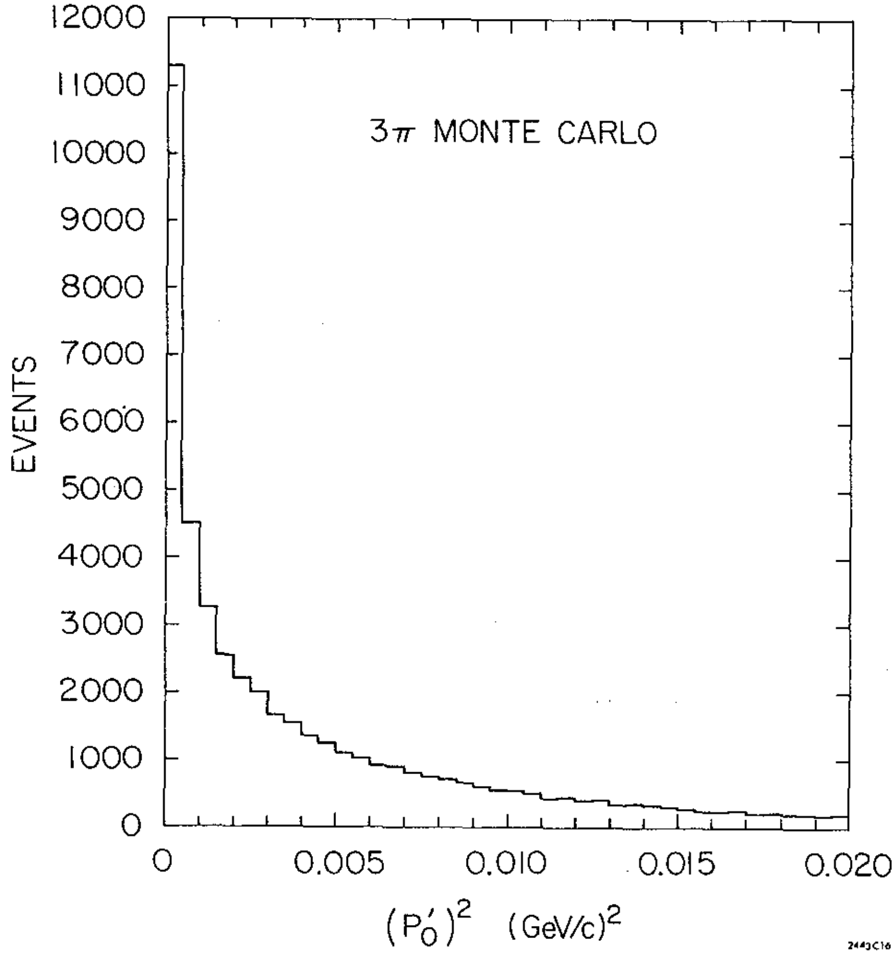

Figure 10 - (P0')² distribution for fake K3pi events.

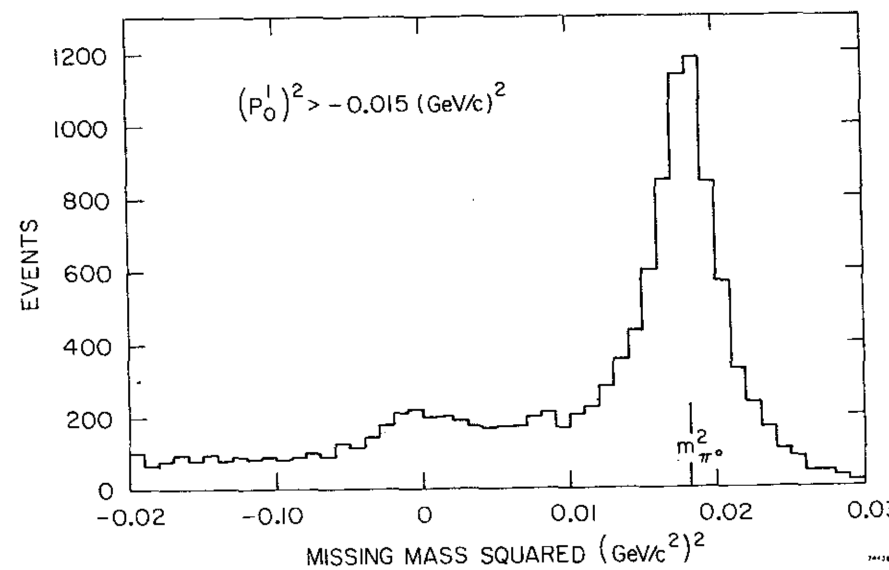

Figure 11 - Missing mass squared distribution of events with (P0')² > -0.015 (GeV/c)².

LEAST SQUARES FITTING AND χ^2 MINIMIZATION

The problem that arises at many stages of the analysis is the determination of the values of a set of n parameters $\{p_\alpha\}$ in order to optimize the agreement between N measurements and a theoretical prediction based on $\{p_\alpha\}$. The most often used procedure in this experiment was the method of least squares fitting, an outline of which is given below.

1. Minimization of χ^2

The quantity which describes the goodness of the fit is:

$$\chi^2 = \sum_{ij} r_i W_{ij} r_j$$

where:

r_i is the residue associated with the i^{TH} measurement, and

W is the weight matrix associated with the residues.

In fitting a set of measured points (x_i, y_i) to an analytic function, the residues would be of the form $(y_i - f(x_i))$: in the case of track reconstruction in space, the residues would be the distances from the measured film and the space curve projected onto film. The weight matrix is the inverse of the variance matrix V of the residues. In many applications V, and hence W, is diagonal, in which case χ^2 is the familiar sum of squares.

Assume that approximate values of the parameters $\{p_\alpha^{old}\}$

are known which give residues r_i^{old}. If the residues are nearly linear in the parameters close to the χ^2 minimum, the residues at the minimum can be written as

$$r_i = r_i^{old} + \sum_\alpha (-q_\alpha^i)(p_\alpha - p_\alpha^{old})$$

where $-q_\alpha^i$ is the derivative of the i^{TH} residue with respect to the α^{TH} parameter evaluated at $\{p_\alpha^{old}\}$. The minimum condition is that the derivatives of χ^2 with respect to each parameter vanish.

i.e. $\sum_{ij} W_{ij} r_i \dfrac{\partial r_j}{\partial p_\alpha} = 0$ for all α.

Expressing r_i as above and using the values of the derivatives at $\{p_\alpha^{old}\}$ leads to:

$$p_\alpha = p_\alpha^{old} + \sum_\beta G^{-1}_{\alpha\beta} v_\beta$$

where:

G^{-1} is the inverse of the matrix G, where $G_{\alpha\beta} = \sum_{ij} q_\alpha^i W_{ij} q_\beta^j$, and

$$v_\beta = \sum_{ij} r_i^{old} W_{ij} q_\beta^j$$

The new values of $\{p_\alpha\}$ can now be used as starting values and the process repeated until the minimum is reached. This iteration is not necessary if the residues are truly linear in the parameters, as would be the case in a polynomial fit for example.

2. The Variance Matrix and the Error Ellipsoid

If $\{p_\alpha^0\}$ are the values of the parameters that minimize χ^2, near the minimum:

$$\chi^2 = \chi^2_{min} + \sum_{\alpha\beta}(p_\alpha - p^o_\alpha)\, G_{\alpha\beta}\, (p_\beta - p^o_\beta)$$

The hypersurface in parameter space defined by $\chi^2 = \chi^2_{min}+1$ is called the error ellipsoid, and the error on p_α (denoted by δp_α) is given by the maximum value that $(p_\alpha - p^o_\alpha)$ can take on the ellipsoid. Using the method of Lagrange multipliers requires that we maximize the quantity

$$(p_\alpha - p^o_\alpha) + \lambda_\alpha\Big(\sum_{\beta\gamma}(p_\beta - p^o_\beta)\, G_{\beta\gamma}\, (p_\gamma - p^o_\gamma) - 1\Big)$$

with respect to all the parameters which are now treated as if they are independent. Differentiating and using the constraint condition to eliminate λ_α gives the result:

$$(p_\alpha - p^o_\alpha)(p_\beta - p^o_\beta) = G^{-1}_{\alpha\beta} \text{ for } (p_\alpha - p^o_\alpha) \text{ maximum.}$$

$$\text{i.e.}\quad (p_\alpha - p^o_\alpha)^2 = G^{-1}_{\alpha\alpha} \text{ or } \delta p_\alpha = \sqrt{G^{-1}_{\alpha\alpha}}\ .$$

Thus the off-diagonal elements of G^{-1} tell how much the other parameters must move away from their values that minimize χ^2 in order to make $(p_\alpha - p^o_\alpha)$ a maximum on the error ellipsoid. $G^{-1}_{\alpha\beta}/(\delta p_\alpha \delta p_\beta)$ is the correlation between p_α and p_β.

The variance of a quantity Q which depends on the parameters $\{p_\alpha\}$ is given by:

$$\delta Q^2 = \sum_{\alpha\beta} \frac{\partial Q}{\partial p_\alpha} G^{-1}_{\alpha\beta} \frac{\partial Q}{\partial p_\beta}$$

3. Convergence Criteria

The question of when to stop iterating the fit must be investigated separately for each application. In some cases it may be enough to quit when the corrections are such that

the predicted change in χ^2 falls below a certain value. This predicted change is

$$\Delta\chi^2 = \sum_{\alpha\beta} \Delta p_\alpha G_{\alpha\beta} \Delta p_\beta$$

where:

Δp_α is the prescribed correction to p_α.

In cases where the residues are rather nonlinear, it may be necessary to actually apply the correction and evaluate the new value of χ^2 before stopping.

4. Goodness of Fit and Relative Weights

Before it is possible to decide whether the fit is good, attention must be given to the weights entering into χ^2. If all the measurements have the same error, an incorrect error assignment only scales χ^2 and the error matrix, but does not affect the convergence or the final values of the parameters (for the same number of iterations). In some cases, however, it may be necessary to give different measurements different weights for some systematic reasons or due to their being completely different types of measurements. The latter occurs in the kinematic fit where the K^0_L momentum, the K^0_L beam angles, and the charged particle momenta are determined differently.

For N measurements and n parameters χ^2 should have a theoretical χ^2 distribution for N-n degrees of freedom. The differential probability distribution is (reference 17):

$$P(\chi^2) = \frac{e^{-\chi^2/2}(\chi^2)^{(m/2)-1}}{2^{m/2}\Gamma(m/2)} \quad \text{for } m=N-n.$$

For large m, the distribution is approximately Gaussian with $\langle\chi^2\rangle = m$ and $\sigma = \sqrt{2m}$. The confidence level or probability for a given value of χ^2 (say χ_c^2) is thus:

$$\text{prob} = \int_{\chi_c^2}^{\infty} P(\chi^2)\, d\chi^2.$$

5. Constrained Fits

It sometimes happens that in addition to minimizing χ^2, the parameters must satisfy certain relations among themselves. Each of these relations (called constraints) reduces the number of free parameters by 1, and hence increases the number of degrees of freedom by 1. In some cases it may be possible to reduce the set of parameters to a smaller set of independent ones and proceed with an unconstrained fit. In many cases (such as kinematic fitting) the choice of certain parameters as "obviously dependent" is not obvicus. Furthermore the constraint equations may be be too complicated to solve for these "dependent" variables. The method of Lagrange multipliers is used to solve the problem.

If the constraints are each expressible in the form $F(\{p_\alpha\})=0$, we minimize the quantity

$$\chi^2 + \sum_i \lambda_i F_i(\{p_\alpha\})$$

where λ_i is an undetermined parameter to be determined from the minimum condition and the constraint equaticns. There is one λ per constraint and the parameters are treated as independent.

The procedure is the same as for the unconstrained fit except that the constraint equations must be linearized as well as the residues. Thus the success may depend critically on the particular formulation of the constraints.

6. Kinematic Fitting

The problem that occurs in this experiment is that of constraining measured track parameters (angles and momenta) to conserve 4-momentum. The parameters have been "measured" by doing an unconstrained fit to minimize the sum of squares of residues on film. This set of parameters {p (meas)} has associated with it a correlated variance matrix G^{-1} which is not diagonal. The adjustment of $\{p_\alpha(\text{meas})\}$ is carried out by minimizing

$$\chi^2 = \sum_{\alpha\beta}(p_\alpha - p_\alpha(\text{meas}))\,G_{\alpha\beta}\,(p_\beta - p_\beta(\text{meas}))$$

with the appropriate constraints. The precise formulation of the constraints is described in reference 20. Note that the residues here are particularly simple functions of the parameters.

Since the number of residues is the number of measured parameters,

$$DF = NP - (NP+NM) + 4 = 4 - NM$$

where:

DF is the number of degrees of freedom,

NP is the number of measured parameters,

NM is the number of unmeasured (missing) parameters, and

the 4 comes from the conservation of 4-momentum.

This shows that the degrees of freedom is given by the number of effective constraints. Thus for the case of $K^0_L \longrightarrow \pi^+\pi^-\pi^0$ we have 3 missing variables (the π^0 3-momentum), hence a 1C fit. For $K^0_S \longrightarrow \pi^+\pi^-$ with 1 missing variable (the K^0_S 3-momentum magnitude if we don't include the timing information) we have a 3C fit. Once the fit is carried out, a new set of parameters $\{p_\alpha\}$ is obtained with a new variance matrix $(G')^{-1}$.

While the value of χ^2 tells whether the fit is good, it does not give any indication about systematic errors in the measurements. One must resort to a study of the so-called stretch plots. The stretch of a parameter p_α is defined by:

$$\text{stretch} = (p_\alpha - p_\alpha(\text{meas})) \;/\; \sqrt{G^{-1}_{\alpha\alpha} - (G')^{-1}_{\alpha\alpha}}$$

It is shown in reference 18 that the stretch should distribute symmetrically about zero with unit standard deviation. 1C fits are not highly enough constrained to provide useful stretch information, but the 3C stretches can be useful for making fine adjustments to certain parameters.

MONTE CARLO METHODS

Monte Carlo techniques were used at practically every stage of the experiment. Although the specific details are discussed in the appropriate chapters, a brief summary of the different applications is given below.

1. Applications

During the design stage of the experiment, the location of the counters was chosen to optimize the the trigger efficiency. In the latter stages of analysis, the precise geometrical efficiency was determined.

Kinematic features of semileptonic decays and other contaminations were studied with fake events. Some of these properties were impossible to determine otherwise.

Fake measurements were used to test the geometry and later to study the effects of measurement errors on kinematic quantities.

Systematic effects were studied by introducing known errors into the fake events and comparing the resultant distributions with the undistorted ones.

2. Mechanics

The generation of fake events consisted of two parts. First a center-of-mass configuration was chosen, and then this was transformed to the laboratory. 3 pi decays were generated uniformly on the Dalitz plot and the events were weighted by the square of the supposed matrix element at later stages. Semileptonic decays were needed to study the effects of contamination. Hence a matrix element appropriate to the vector interaction with reasonable parameters was taken and events generated accordingly. All events were given a random orientation in space (in the c.m.). The decay vertex of the event was chosen randomly in the determined fiducial volume, and the K_L^0 momentum was taken either fixed or according to a spectrum depending on the application. A Lorentz transformation was carried out and the event was rotated according to the appropriate beam angle.

SCANNING

Approximately 2,500,000 pictures (in three views for a total of 7,500,000) were taken during the experiment, 20% of which were analyzed at SLAC. The remaining 80% of the data are being analyzed at Brookhaven National Laboratory. Thus the data base considered here consists of approximately 50 rolls of film with 10,000 pictures on each. Every fifth roll was included in the sample so that changes in various conditions over the course of the experiment could be studied.

1. Purpose and Procedure

The trigger for the experiment was designed to be highly efficient for detecting K_L^0 decays, with the not unexpected result that the event rate was about 20% of the trigger rate. Thus the main purpose of scanning the film was to find the event candidates and record their presence for subsequent measurement. Each scan table had three projectors (one for each view of the chamber). The film was projected upwards against two mirrors which reflected the light back down onto a horizontal white table. The magnification was about 20 for a total demagnification from space of about 4. A frame was considered to have contained an event if the scanner saw a positive and a negative particle track which originated from a common decay vertex within the streamer chamber's sensitive volume. Due to their topology, events were also referred to as V's. When an event was found, the pertinent information was coded onto a form and was later punched onto IBM cards. The data on the cards was then transferred to magnetic tape. Two independent scans were made (before and after the first measurement pass).

2. Scan Record

The scanner entered the roll and frame number, the date, his own ID number, as well as a description of the event according to a set of instructions. The most important information from the scan was the description of the particles' behavior on passing through the lead oxide plates. Each particle had a one digit code telling how many secondary particles emerged from the plate, and a one digit code intended to allow a partial identification of the particle. These "track type" codes are explained in Table 1. Each event was given an "event type" code 2ij where i and j were the "track type" codes of the positive and negative tracks respectively.

Other information which was coded included the overall event quality (faintness of tracks, presence of flares, etc.), and the possible existence of extra tracks in the picture which could affect the time-of-flight determination. The former was not used however, since the ultimate decision on the

measurability of the event was left to the measurer when the event was on the measuring table.

3. Scanning Efficiency

The data sample consisted of 101,192 events which had shown up in at least one scan, had a good PDP-9 record, and had only one event in the frame. Since two independent scans were made, it is possible to estimate the number of events lost due to their not having been scanned. Assuming only random losses, we have:

$N(L) = (N(1)N(2)-N(12)N(F))/N(12)$ and

$eff = N(F)N(12)/N(1)N(2)$

where:

$N(L)$ is the number of events lost,

$N(1)$, $N(2)$ are the numbers of events found in scans 1 and 2 respectively,

$N(12)$ is the number of events found in both scans 1 and 2,

$N(F) = N(1) + N(2) - N(12)$ is the total number of events found in at least one scan, and

eff is the overall scanning efficiency.

These numbers are given in Table 2 for the complete sample as well as for some subsamples. In particular, the scanning loss for events subjected to the standard fiducial volume cut (described in a later chapter) is completely negligible

3. Event Type and $(PO')^2$

While the event type from scanning and the value of $(PO')^2$ were not used directly in the decay mode separation, they were used during early stages of the analysis. $(PO')^2$ distributions for a few event type selections are shown in figure 12.

a) The plot for all events shows the separation between the 3 pi decays and the semileptonic modes.

b) Requiring type 211 eliminates virtually all the Ke3 decays, leaving Kmu3 and K3pi in the approximate ratio of 2:1.

c) Type 212, 213, 221, and 231 should give a rather pure Ke3 sample.

Table 1

Track Type Codes Used in Scanning

0 - No secondaries.

1 - The particle goes through with no energy loss or scatter

2 - The particle loses energy but does not scatter.

3 - Electron shower. All secondaries of lower energy than the primary, and no scatters.

4 - Pion interaction. At least one secondary is at some perceptible angle to the primary.

5 - Energy loss, charge reversal, no scatter.

6 - Particle fails to reach plate. Usually due to its low momentum.

7 - Defies description in terms of other codes. Includes decays in flight.

8 - Particle passes through the slot between the right and left plates.

9 - Behavior is obscured by a flare behind the plate.

Table 2

Scanning Results and Efficiencies

	all events	pass geometry	fiducial volume cut
N(1)	96653	90224	60564
N(2)	96375	90068	60666
N(12)	91836	86704	59824
N(F)	101192	93588	61405
N(12)/N(F) (%)	90.106	92.644	97.425
N(L)	238.08	136.57	11.42
eff (%)	99.765	99.854	99.981

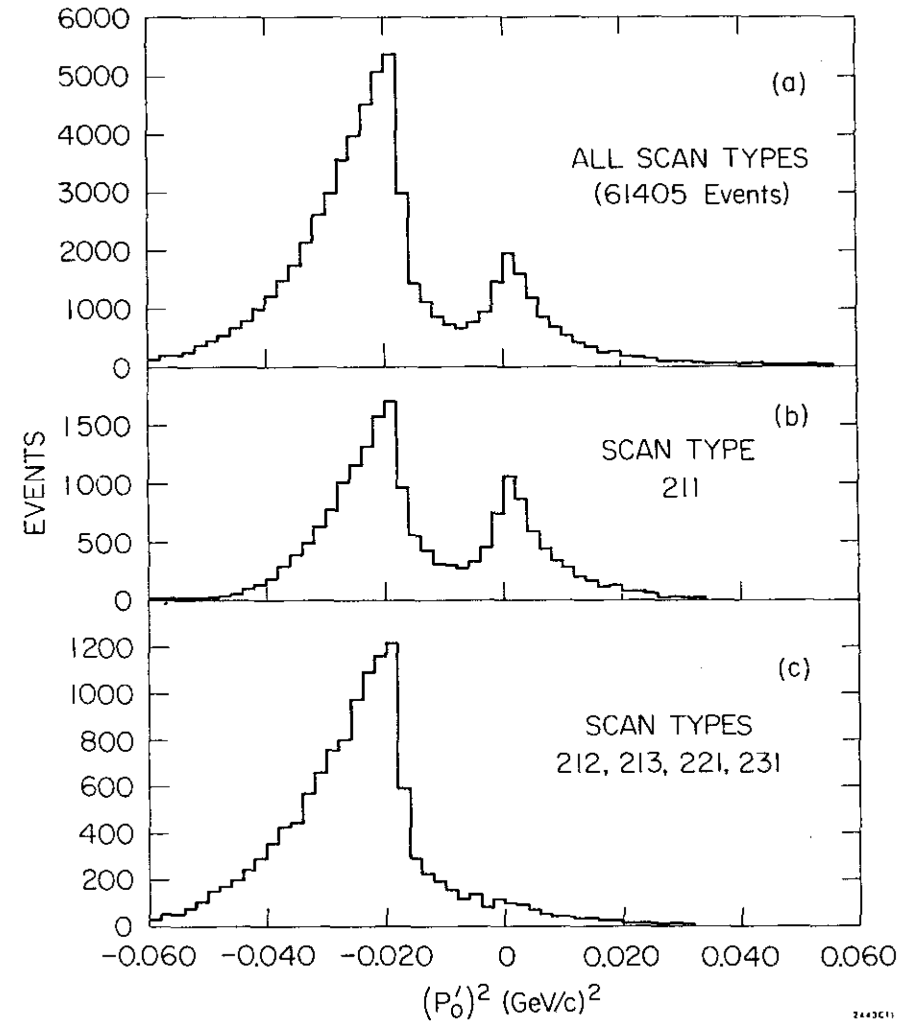

Figure 12 - (P0')² distribution for event type cuts.

OPTICAL CONSTANTS

1. Formulation of the Fit

The term "optical constants" refers to the camera positions, focal distances, optical distortions, camera tilts, etc. as well as the positions of the fiducials in space. All these parameters were measured as well as possible - camera and fiducial positions were surveyed; lens parameters were measured on an optical bench; tilts were held tc design values which were known. In all there were 129 parameters to consider.

The fiducial positions on film were measured in all three views for about forty adjacent frames on a given roll. The results were matched and averaged to provide one "best" set of measured fiducials. Then the parameters were adjusted to minimize the quantity:

$$\chi^2 = \sum_i w_i (v_i(\text{meas}) - v_i(\text{proj}))^2 + \sum_\alpha u_\alpha (p_\alpha(\text{meas}) - p_\alpha(\text{fit}))^2$$

where:

p_α(meas) is the measured value of the $\alpha^{\underline{th}}$ optical constant,

p_α(fit) is the value of the $\alpha^{\underline{th}}$ optical constant which is adjusted to minimize χ^2,

v_i(meas) is the $i^{\underline{th}}$ coordinate on film of the fiducial (the index i refers to fiducial, view, and x or y direction in the film plane),

v_i(proj) is the coordinate calculated from the optical constants $\{p_\alpha(\text{fit})\}$, and

u_α and w_i are appropriate weights.

The term in χ^2 containing the measured values of the parameters had the effect of putting a partial constraint on them. This was desirable on two grounds. First, it was appealing to have all the measurements (parameters as well as film points) on a more or less equal footing as input to the program. More important however was the fact that serious numerical difficulties were avoided. If the parameters had been free to float without any constraint, χ^2 would have been invariant under rigid rotations and translations of the whole optical system, resulting in a singular matrix.

The measured values of the parameters were used as initial values, and corrections were obtained by the standard least squares minimization technique. The normal equations were built up and the resultant 129 by 129 matrix was inverted. The process took about four iterations to converge. The output also included a table of the film coordinates of the five large fiducials, which was used in the event reconstruction to register the film. For this purpose the measured values (rotated and translated to the optical coordinate system) were used rather than the fitted values.

2. Comparison of Different Sets

Fiducial measurements were made on film taken at various times during the experiment, and optical constants were obtained. These sets were compared for consistency in three ways.

The most convincing approach involved processing actual events with different sets of optical constants in the geometry program and looking for differences. In particular, optical constants determined from film taken at the beginning and the end of the experiment were used to process about 1000 events at each of these extremes. Differences of various quantities computed on the same events due to the two sets of optical constants were histogrammed. Both raw geometry output (momenta, angles, vertex) and kinematic quantities derived from the geometry output (K_L^0 momentum, $(PO')^2$, π^0 center of mass energy) were checked. No significant effect was found - the differences were typically less than 10% of the errors on the quantities.

The second method involved matching the different sets of matched and averaged fiducials and seeing how well they agreed. The rms deviation of the fiducial measurements on adjacent frames was about 6 μ (giving an error on the mean of the order of 1 μ), whereas the rms of the various sets

among themselves was typically 2 μ. A more relevant scale for comparison was set by the fact that typical track points had an rms of 10 μ, which was considerably greater than the possible 2 μ systematics due to choosing one set of optical constants over another.

The third method involved a mere visual inspection of the optical constants generated with the different sets of matched and averaged fiducials. It was noted that the various parameters agreed within their errors.

Since all three considerations indicated that one set of optical constants adequately described the data, six sets of fiducial measurements uniformly spanning the data were averaged and a single set of optical constants was obtained. Some of these values are shown in Table 3.

Table 3

Values of Some of the Optical Constants
Used in the Event Reconstruction

	Camera 1	Camera 2	Camera 3
x-coordinate (m)	0.5134±.0014	0.5128±.0014	1.9811±.0018
y-coordinate (m)	0.5151±.0013	-0.5420±.0013	-0.0150±.0009
z-coordinate (m)	4.0386±.0065	4.0398±.0065	4.0427±.0065
focal length (mm)	52.197±.076	52.315±.077	52.324±.076
distortion parameter (m^{-4}) (c/f^5)	-73458±1211	-65349±1199	-71464±1025

1. Measuring

In order to determine the track parameters in space (momenta, angles, vertex position) it was first necessary to digitize the tracks on film and then to process the film points through a geometrical reconstruction program. In all three different types of measuring machines were used on the data.

The SPVB (SP5B) was basically a converted scan table outfitted with an image plane digitizer having a least count corresponding to 2.6 μ on film. The measured points were written on magnetic tape by a Kennedy Incremental Tape Drive which was connected to the machine.

The NRI was a film plane digitizer with a least count of 1 μ. It was on-line to a small computer (EMR 6020) whose function was to request the tracks and fiducials in the proper sequence, and to write the data on magnetic tape.

The Hummingbird III (HB3) was a CRT digitizer which was on-line to the IBM 360/91 and operated in a semi-automatic mode. The exposed parts of the film were displayed on a television screen, whereupon the measurer light-penned the tracks, enabling the software to accurately determine the track positions on film. Portions of the track were fitted to arcs and pseudo-measured points were constructed.

The output from the three machines was very similar. Aside from minor format differences, the Hummingbird data was distinguished from the rest by having 5 measured fiducials instead of 3. An average of 7.5 points per track per view was typical for all the machines.

2. The Geometry Program

The output tapes from the measuring machines were processed through the computer program SYBIL. An earlier version of SYBIL has been documented[19], but since the program has been completely rewritten, its main features will be outlined here.

The first step in the analysis involved registering the film. The measured fiducials were matched to the values obtained from the optical fitting program. The effects of lens distortions and any tilts of the film plane relative to the optic axis were then removed by undistorting the track points, thereby allowing the use of ideal optics in subsequent computation.

The parameters initially used to describe a track were the cartesian coordinates of the beginning of the track (first

measured point), the inverse momentum, and the azimuth and latitude of the track at the first point. Initial estimates of these quantities were made by doing a two view reconstruction in space. Measured points in one view were projected onto fitted circles in another view to obtain pseudo-corresponding points. Due to the nature of this calculation, the two points (the measured point and its pseudo-corresponding point) gave rise to rays which were guaranteed to intersect in space. Once this procedure had been carried out with all possible pairs of views, the generated space points were fitted to a helix.

In general there were two vertex candidates for an event corresponding to the two points of closest approach of the helices. The final fitting was such that a wrong initial estimate of the vertex tended to give an end result that was wrong. Experience showed that the two view helices were simply not accurate enough for the critical vertex determination. Hence a preliminary fit for the parameters was done on each track individually using the helix values as first estimates. The fitted single track parameters were then used to make the first estimate of the vertex location for the event. The parameter set from that point on consisted of the vertex coordinates for the event and the inverse momentum and angles for each track. The initial values were then adjusted to minimize the quantity:

$$\chi^2 = \sum w\,(\mathrm{res})^2$$

where:

the sum is over all the measured points in all views,

w is the weight given by 1/(setting error)^2, and

res is the distance on film from the projected track to the measured point.

The minimization was done in the film plane because the errors there were expected to be reasonably gaussian in nature, being due in large part to random measuring error.

The particle trajectory in the magnetic field was defined by the set of six differential equations with the independent parameter s, the arc length along the track:

$$d\hat{u}/ds = (c/p)\,\hat{u} \times \vec{B}$$

$$d\vec{x}/ds = \hat{u}$$

where:

$\hat{u}$ is the unit vector tangent to the trajectory,

$\vec{x}$ is the position vector along the trajectory,

$\vec{B}$ is the magnetic field,

p is the momentum of the particle with the sign given by the charge of the particle, and

c=.02997925 for B in kilogauss, p in GeV/c and s in meters.

These equations were numerically integrated through the inhomogeneous magnetic field using a third order Runge-Kutta method, leading to the evaluation of the residues and their

derivatives with respect to the parameters. These were fed into a fitting program which prescribed corrections to the parameters. The corrections were applied and the whole integration and fitting procedure was repeated with the new values of the parameters. The process was terminated when the corrections lay within the error ellipsoid, i.e. when the corrections were such that χ^2 would change by less than 1 if they were applied.

In the process of fitting the parameters, the matrix representing the normal equations had to be inverted. The inverted matrix was just the full correlated variance matrix, and was written out on tape with the parameters themselves. The full variance matrix was necessary both for kinematic fitting and for calculating the variance of more complex kinematic quantities.

Since the intrinsic measuring accuracy varied from measurer to measurer, the variance matrix was scaled before the kinematic fit. The average standard deviation was computed for each measurer, and the variance matrix for each of his (her) measured events was multiplied by the square of this quantity. The values of average standard deviation ranged between 0.56 and 1.24 with an overall mean of 0.87. Since the setting error used to process the measurements was 10 μ, this corresponded to a typical accuracy of 8.7 μ on film.

3. Geometry Failures

Of the 101,192 events that were to be measured (frames with two V's had been excluded), 7604 failed to give a good geometry record. The reasons for this are shown in Table 4. The operator rejects due to flares and spirals, and the reconstruction failures were suspect as possible sources of bias, and required further consideration.

Events with a low momentum track which spiralled, making measurement impossible, were viewed on the scan table and it was concluded that virtually all of them were Ke3 decays. This was due to the low momentum of the spiralling track (10-100 MeV/c which was kinematically forbidden in 3 pi decays) and the absence of observable energy loss by ionization which would have been present for picns or muons.

Events whose measurement was rendered impossible by the presence of a flare in the picture were found tc present negligible bias for the 3 pi analysis. In apprcximately 80% of the cases, the flare was unrelated to the event configuration. The majority of these events had their vertex in the downstream half of the chamber and would have been removed by the standard fiducial volume cut described in a later section. In the case of the other 20%, it was possible that the flare was obscuring a very low momentum spiralling track, or that it was due to a very steep track.

Both of these configurations did not occur in 3 pi decays.

The number of events that SYBIL was unable to reconstruct (3495) was at the level expected had there been no remeasurements. This was due to a minor technical reason, since there were in fact two remeasurement passes. The remeasurements were done on the basis of what had failed an early version of SYBIL, and by the time the new version was written, it was not possible to remeasure the events that failed it. (After remeasurement, only about 700 events had failed reconstruction with the old SYBIL). The study of the reconstruction failures proceeded along two lines.

50,000 3 pi and 20,000 semileptonic decays were generated with the observed K^0_L momentum spectrum as described in the previous section on Monte Carlo methods. To improve the sensitivity of a later study of the 1C kinematic fit, the semileptonic events were generated with $(P0')^2$ above -0.020 $(GeV/c)^2$. Fake film points were obtained by integrating the charged particle trajectories through the magnetic field and projecting points onto the film planes of the three cameras. After the appropriate optical distortions had been applied, these "ideal" film points were given gaussian errors to simulate the real data. These "measurements" were then run through SYBIL. Failures were at the 3% level, and no biasing structure was found in them. The other approach involved running the failed measurements from the real data through a version of SYBIL where various convergence criteria, etc. had been relaxed. Virtually all the events could be forced to pass, and no apparent distinguishing features were found.

The 1075 fiducial failures were due to the fact that the old version of SYBIL allowed bad fiducial measurements in one view whereas the new version did not. Hence the events with badly measured fiducials were in general not remeasured.

Table 4

Results of the Geometry Program

101192 - Total		
93588 - Pass geometry		
3495 - Fail reconstruction		
1075 - Fiducial failure		
2866 - Not measured (operator reject)		
	1389	event obscured by flare
	683	no event in frame
	609	low momentum track spirals making measurement impossible
	125	tracks too faint
	36	two events in frame
	24	bad film
168 - Other		

SPECIAL RUNS

Over the course of the data taking, certain calibration runs were made wherein particles other than K^0's were run into the chamber.

1. Regenerated K^0_S.

The regenerator consisted of an 8" thick block of the lead oxide and epoxy mixture used for the particle identification plates in the chamber. It was periodically moved into the beam just outside the front wall of the chamber. The trigger was modified to require an A-B coincidence on both sides of the chamber. Only V's with vertices in the first third of the chamber were measured to further enhance the small K^0_S signal. The K^0_S's were used to make fine adjustments to the values of the beam angles.

2. Muons.

Muons were run into the chamber by turning off the sweeping magnets and taking the anti counters out of anticoincidence with M_o. Also M_o' was delayed by 5 ns to ensure reliable triggering on nearly v=c particles (see section on counter logic). The muon events were used to determine preliminary values of the timing constants.

3. Straight Muons.

Muons were run into the chamber with the streamer chamber magnet off for beam angle studies. However the optical constants were different for the no-field condition, so the beam angles determined in this way were not used.

CHAPTER IV

THE 1C KINEMATIC FIT

The separation of the various decay modes of the K_L^o to obtain a complete and uncontaminated sample of 3 pi decays was probably the most critical part of the analysis. The measurement errors had the effect of making some 3 pi events unphysical and the time-of-flight information was difficult to incorporate in a meaningful way. The kinematic fitting program FIT73[20] was used to process the geometry output and extract the information present as completely as possible. Before the data could be run through the kinematic fitting program, the beam angles had to be determined and the time-of-flight formulated. Subsequent to the fitting, cuts on vertex location, K_L^o momentum, and fit probability were made. Events that had acceptable fit probabilities for the 3 pi and semileptonic hypotheses were given special consideration. Details of the above are given in this chapter.

TIMING ANALYSIS

The procedure of separating the decay modes using the 1C fit depended critically on the time-of-flight determination of the K_L^o momentum. It was important to determine the time itself as accurately as possible, and in order to make the 1C meaningful, it was also necessary to understand the error on the time.

1. ADC Calibration Curves

The hardware and light diode calibration procedure is described in the section on counter electronics. The formulation of the data in a form suitable for computation is discussed below.

Cable lengths (delays) from 0-38 ns in increments of 3 or 5 ns gave ADC channel readings over the range 0-170. For each time in a given calibration run, the ADC channel reading for each counter was histogrammed and averaged. Points more than 3 standard deviations from the mean were discarded and the mean and standard deviation were recomputed. A typical rms deviation was 2 channels, corresponding to an error on the mean of .07 channels for 1000 pulses.

The resulting "channels vs. nanoseconds" plots were smoothed out by fitting a 4^{TH} order polynomial to the central region. The flat regions at the edges were left alone. The rms of this fit was typically less than 0.2 channels. A table of times corresponding to ADC readings of 0,10,... 170 for each counter was prepared using a four point quadratic interpolation. The tables from five of the eleven calibration runs were required to properly give the ADC channel-to-time correlationn over the course of the experiment. The breaks corresponded to actual breaks in data taking (due to accelerator shutdown) and tc any changes in the counter or ADC conditions.

The 5 tables were stored as part of a closed subroutine which gave a time in nanoseconds for any ADC channel value. A linear interpolation was used and the zero of time was arbitrarily set to correspond to a channel reading of 80.

2. Timing Constants - Formulation

Consider a single counter. The reading of the time ADC converted to nanoseconds does not directly give the K^0 time-of-flight. Recalling that a large ADC reading signifies a small time-of-flight, we have the relation:

$$t' - t(ADC) = T + s/v + F(A,x)$$

where:

t' is an overall additive constant which includes all the cable lengths, electronics delays, etc.,

$t(ADC)$ is the ADC time,

T is the K^0_L time-of-flight to its decay vertex,

s is the distance the charged decay particle travels from the decay vertex before hitting the counter,

v is the speed of the charged particle as determined from its measured momentum and mass assignment, and

$F(A,x)$ is a function of the amplitude ADC reading and the x-coordinate of the particle hit on the counter as described below.

The term $F(A,x)$ must take two main features into account. The transit time of the light in the scintillatcr can be expressed as a term proportional to x, the arbitrariness of the origin being absorbed into t'. The speed of light in the plastic is effectively reduced since internally reflected light as well as direct light goes into making a pulse above the threshold of the discriminator. Because this reduction is more pronounced for small pulses, a term proportional to A.x is also included. An amplitude correction due to the fact that small pulses take longer to rise to threshold is expressed as a quadratic in (A-Amax) where Amax is the reading at which the ADC saturates. Thus:

$$F(A,x) = n'x/c(\cos\theta) + a'(A-A_{max}) + a''(A-A_{max})^2 + bAx$$

where:

n' is the effective index of refraction,

x is the hit position on the counter,

c is the speed of light in vacuum,

θ is the angle between the direction of light travel in the counter and the negative x-axis,

a' and a" are the amplitude correction coefficients, and

b is the coefficient of the A.x term.

The quadratic in A-Amax was not a suitable correction for counter hits with a saturated amplitude ADC reading since the exact amplitude was not known. A constant correction was calculated separately for such hits.

3. Timing Constants - Preliminary Determination

The parameters required for each counter were the overall constant t', the index of refraction n', the A.x coefficient b, and the amplitude correction coefficients a' and a". The determination of these constants was a long iterative procedure, since the selection of the data to fit for the constants was itself dependent on the timing information. The C and D counter information was not considered until the final stage due to its more complicated nature.

Preliminary values for t' were determined from the muon measurements assuming a value of 1.9 for n' and no amplitude dependent terms. These values were then used to select a small number of 3 pi decays. Events with positive $(P0')^2$ and straight through tracks on both plates (scan type 211) were written out if the timing from the four counters had an

rms deviation from the mean of less than 2.5 ns. A selection of about 300 events whose timing agreed well with only one of the 3 pi 0C solutions was made by hand. They were run through a least squares fit and new constants computed. While these constants were an improvement, they suffered from certain biases. The sample of events was selected on the basis of good agreement to begin with, and there was no provision to include more events in the fit at later stages. In particular, the amplitude correction parameters came out consistent with zero since the events already agreed well with the 0C solutions before the fit. Furthermore the method was not suitable for large numbers of events. Nevertheless the constants were good enough for starting values in the subsequent step.

In order to make the input of the timing fit as independent of the starting values as possible, the mode identification was made without the timing at all. Ke3 decays were selected by requiring an electron shower or energy loss on one plate, a straight through track on the other (scan types 212, 213, 221, and 231), and a value of less than $-0.015\ (GeV/c)^2$ for $(P0')^2$.

Events included in the fit were required to have at least three of the four counter times within 3 ns of their mean. The 0C solution nearer the average counter time was chosen and the times of the counters hit by the pion track were transmitted to the fitting program if the agreement was better than 5 ns. The only amplitude dependence included was a term linear in (A-Amax).

The fit was linear and iteration would not have been necessary if all the selected Ke3 events had been included. This was not the case, however, and the confidence in the procedure came from the observation that more events met the inclusion criteria on each successive iteration. The rms of 1.7 ns per counter included the geometry errors and corresponded to an intrinsic rms per counter of about 1.2 ns. The constants obtained from this fit were used in the first pass of the 1C kinematic fit. The sample of unique 3 pi events was then used for the final timing fit with the full amplitude correlations.

4. Timing Constants - Final Determination

The unique 3 pi events were divided into five groups (corresponding to the five ADC calibration ranges), and a separate fit was done for each. The residue for a given counter in an event was of the form:

t(from 1C fit) - t(from ADC's)

and was transmitted to the fitting program if the amplitude ADC was below saturation. After the fit, the center of the distribution of the untransmitted residues was determined and taken as the constant amplitude correction for counter

times with a saturated amplitude ADC. As well as the five parameters (t', n', b, a', and a") for each of the sixteen counters, the flight path from the target was fitted, for a total of 81 parameters.

The final values for the parameters, the rms deviations for each counter with and without a saturated amplitude ADC, and the constant amplitude corrections were stored as part of the 1C fitting package. Typical rms values for the counters are shown in Table 5. The generally inferior quality of the C and D timing as compared to the A and B timing is attributable to the inaccuracies in the extrapolation of the tracks after the plates, and to the large number of extra tracks hitting the C and D counters.

A weighted average was used as input to the 1C, and the input error was given by:

$$\sigma = 1/\sqrt{\sum_i w_i}$$

where w_i is the weight (1/rms²) of the i^{TH} counter in the event. The distribution of σ for good 3 pi events is shown in figure 13. A high momentum K_L^0 had fewer counter hits on the average, and hence tended to have a higher timing error.

Table 5

Typical Values of Counter Time rms Deviations Resulting from the Timing Fit

counter	rms without saturated amplitude ADC (nanoseconds)	rms with saturated amplitude ADC (nanoseconds)
A1	1.04	0.96
A2	0.94	1.05
A3	0.99	0.98
A4	1.09	1.02
B1	1.12	1.23
B2	1.14	1.13
B3	1.16	1.24
B4	1.09	1.20
C1	1.20	3.19
C2	1.55	3.71
C3	1.35	2.25
C4	1.21	1.68
D1	1.28	3.75
D2	1.37	2.35
D3	1.41	2.59
D4	1.17	1.94

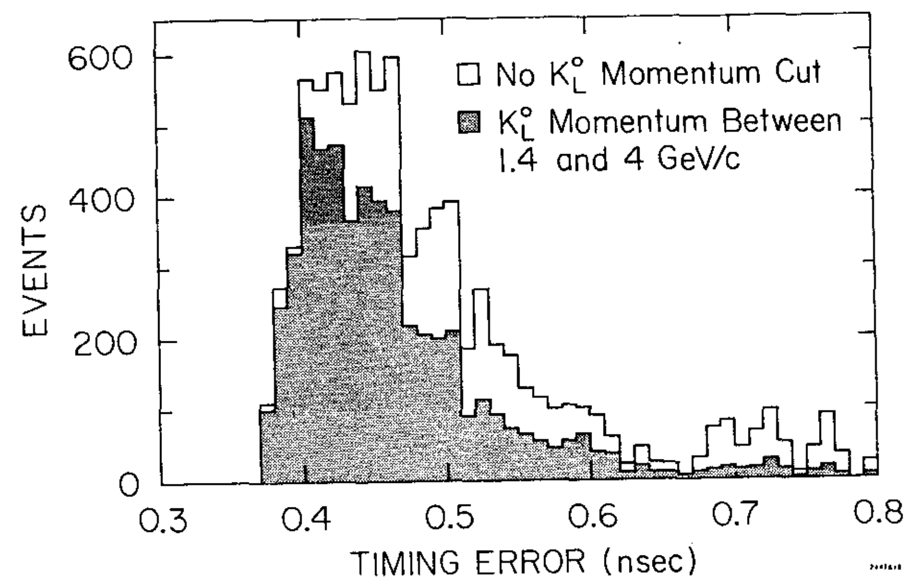

Figure 13 - Timing error distribution.

BEAM ANGLE DETERMINATION

Since the beam particles went through a lead filter before the first collimator (13C1), they were treated as if they originated from 13C1 rather than from the target. The angle at the chamber subtended by 13C1 was .45 mr vertically and .86 mr horizontally (1.5" X 2.875" at 85 m).

Once a central beam direction had been established, the beam angles for a given event were corrected for the position of the decay vertex in the chamber. The angles λ (latitude) and ϕ (azimuth) were given by:

$$\lambda = \lambda^o + z/(x-x^o)$$

$$\phi = \phi^o + y/(x-x^o)$$

where:

x, y, and z are the vertex coordinates,

x^o is the x-coordinate of 13C1 (-85 m), and

λ^o and ϕ^o are the central values of the beam angles, the determination of which is described below.

Since the beam at the chamber was 14 cm wide and 19 cm high, the corrections were of the order of 1 mr or less.

Preliminary values of λ^o and ϕ^o were obtained from the distributions of $(\lambda - z/(x-x^o))$ and $(\phi - y/(x-x^o))$ for the vector sum of the charged particle momenta in the regular K^o_L data. The distributions were wide (FWHM of 50 mr) but very symmetric about their symmetric values. The median was

used to define the central value since the average was sensitive to a small number of events with anomalously large angles. The statistical errors were of the order of .2 mr.

These values of λ^o and ϕ^o were used in a 3C fit on the regenerator data and gaussian ideograms of the fitted beam angles were plotted. The peak values were taken as the nominal beam angles for the 1C fit. The values were:

$\lambda^o = .00617 \pm .004$

$\phi^o = .00226 \pm .003$

EVENT SELECTION.

1. Fiducial Volume Cuts

The final sample of events was subject to the following vertex cuts:

$0.1 < x < 1.1$

$-0.07 < y < 0.07$

$-0.065 < z < 0.005$ or $0.055 < z < 0.125$

where the coordinates are in meters. This reduced the number of events from 93588 to 61405. The vertex distributions before and after the cut are shown in figures 14 and 15.

The rejection of events on the basis of vertex coordinates was dictated by several factors. The size of the collimators and the septa defined the beam profile in the y-z plane. K^0_L's whose vertices fell outside the edges of the main profile could be expected to have undergone nuclear scattering before entering the chamber. It was also necessary to remove events whose vertices had x-coordinates at both extremes of the chamber. The scan efficiency was lower at the beginning of the chamber due to the difficulty of deciding whether an event was just inside or just outside the inner surface of the wall. The trigger efficiency was

found by Monte Carlo studies (described in another chapter) to fall quite sharply for events with vertices above 1.1 m in x in a manner consistent with the observed x distribution. Also, due to their shorter track lengths, events above 1.1 m tended to have momenta that were not as well measured. Another very important effect of the fiducial volume cut was to remove certain classes of contamination as described in a later chapter.

2. Probability Cuts

While the K^0_L angles and the charged particles' inverse momenta and angles could be expected to have reasonably gaussian errors, the K^0_L inverse momentum could not. This was because the time-of-flight had normal errors, and the momentum was a rapidly varying non-linear function of the time-of-flight in the relevant range. To avoid the systematic shift (to lower K^0_L momentum) that would have resulted from fitting in inverse K^0_L momentum, the fitting program (FIT73) did the fit in terms of time directly.

The geometry output, the K^0_L angles, and the timing information, each with the appropriate errors, were fed into FIT73, and a probability (confidence level) for each of the five 3-body decay hypotheses was obtained. An examination of the probability distributions showed a low probability spike below 8% (see figure 17). This included Dalitz pairs, nuclear interactions, gamma conversions, and K_L^0 decays with spurious timing, as well as the 8% of the good events which just happened to have probability under 8%. Since there was no way to distinguish on an event-by-event basis, a probability cut was dictated. The events that were rejected in this way represented an unbiased sample.

3. Momentum Cuts

The observed K_L^0 momentum spectrum is shown in figure 16. Approximately 1/3 of the data sample was removed by a K_L^0 momentum cut. The small number of events below 1.4 GeV/c was rejected to eliminate cases where the timing of the master trigger (MT) was not determined by the timing pulse (T). Events above 4 GeV/c were removed from the data sample for two main reasons. The trigger loss was starting to become non-negligible above 4 GeV/c (see figure 20), and keeping these events would have required corrections to the data that were larger than desired. More important however, was the fact that the confusion in separating the decay modes became large above 4 GeV/c. This was due to the quadratic dependence of the K_L^0 momentum error on the K_L^0 momentum.

4. Determination of Selection Criteria

Once the fiducial volume, 3 pi fit probability, and K_L^0

momentum cuts had been applied, the sample consisted of 5432 events. 91 events (1.7%) had a semileptonic probability that was higher than the 3 pi probability and a total of 221 events (4.1%) had an acceptable semileptonic probability (above 8%). Virtually all of these potentially ambiguous events had 3 pi fit probabilities below 25% and K_L^0 momenta above 3.5 GeV/c.

This problem of ambiguous events was studied with the Monte Carlo events described in the previous section on geometry failures. The error on the time-of-flight was obtained by studying the timing errors of the real data for different trigger configurations and vertex positions. This was then incorporated with the geometry (SYBIL) output of the fake events and run through FIT73.

The 3 pi events all fit the 3 pi hypothesis and their probability distribution showed no low probability spike. Approximately 0.7% of the 3 pi events with a good 3 pi fit (above 8%) had a semileptonic fit probability which was also above 8%. In 0.3% of the 3 pi events the semileptonic probability was higher than the 3 pi probability. When the semileptonic event samples were normalized for the $(P0')^2$ cut involved in their generation, 0.02% of the Ke3 and 0.08% of the Kmu3 events had a 3 pi fit with a probability above 8%. In about 65% of these cases the 3 pi fit probability was higher than the fit probability for the correct semileptonic hypothesis. As in the case of the real data, the ambiguous events had low probabilities (below 25%) and high K_L^0 momenta (above 3.5 GeV/c).

This lack of correspondence between the real data and the Monte Carlo events was not surprising since the real data had certain non-gaussian characteristics that were impossible to simulate in the Monte Carlo study. The most logical selection method was to choose events whose 3 pi probability was higher than the semileptonic probability. However the other two possibilities (events with a good 3 pi fit without regard to the semileptonic fit, and events with a good 3 pi fit and no good semileptonic fit) were also reasonable, albeit less appealing.

Thus the samples chosen by all three criteria were retained for the final analysis, and differences in the extracted parameters were used to estimate systematic errors due to fit loss and semileptonic contamination. Figure 18 shows the $(P0')^2$ distribution of the events whose 3 pi probability was higher than the semileptonic probability. Also shown is the $(P0')^2$ distribution for events with a semileptonic fit probability above 8% and a 3 pi fit probability below 8%.

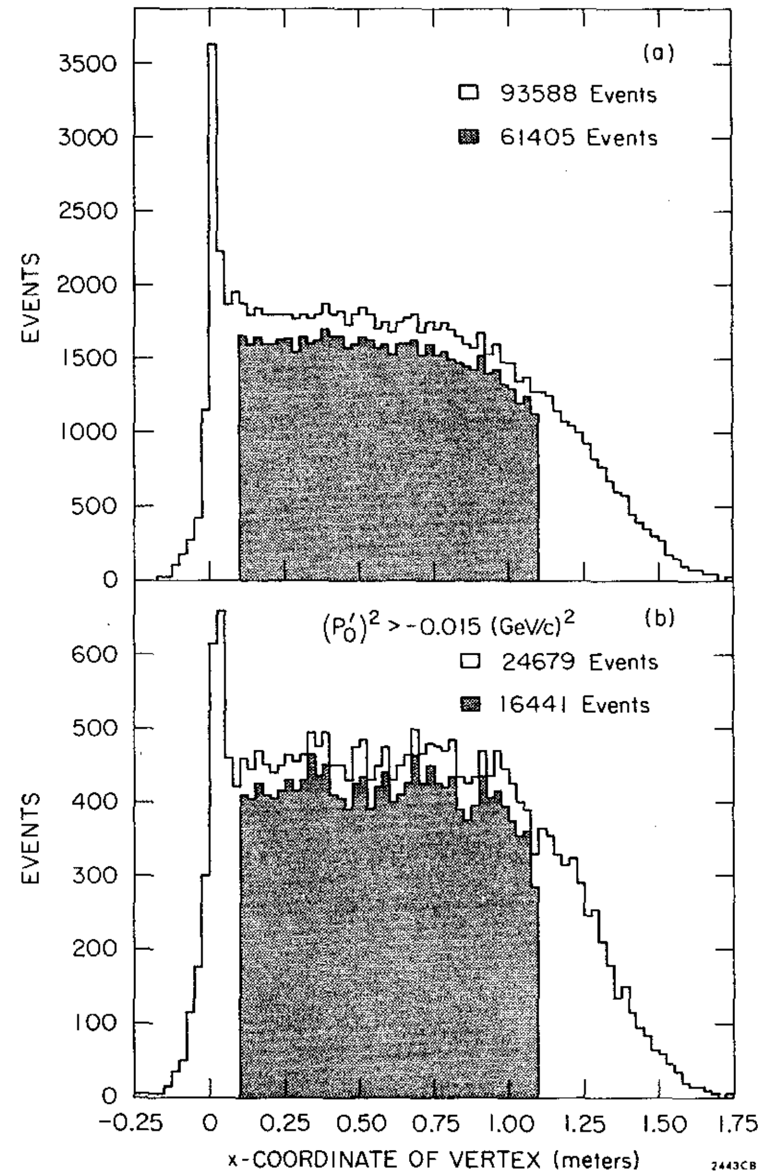

Figure 14 - Distribution of vertex coordinate along beam.

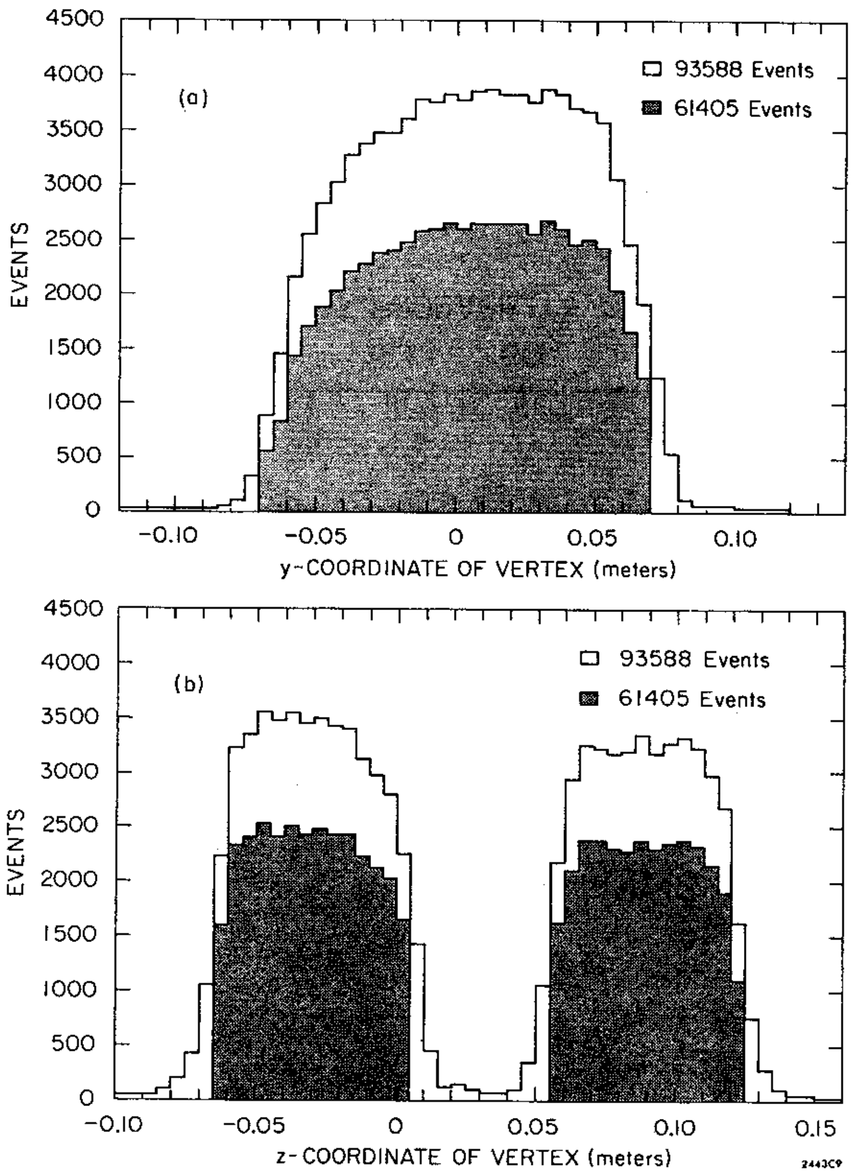

Figure 15 - Distribution of vertex coordinates transverse to beam.

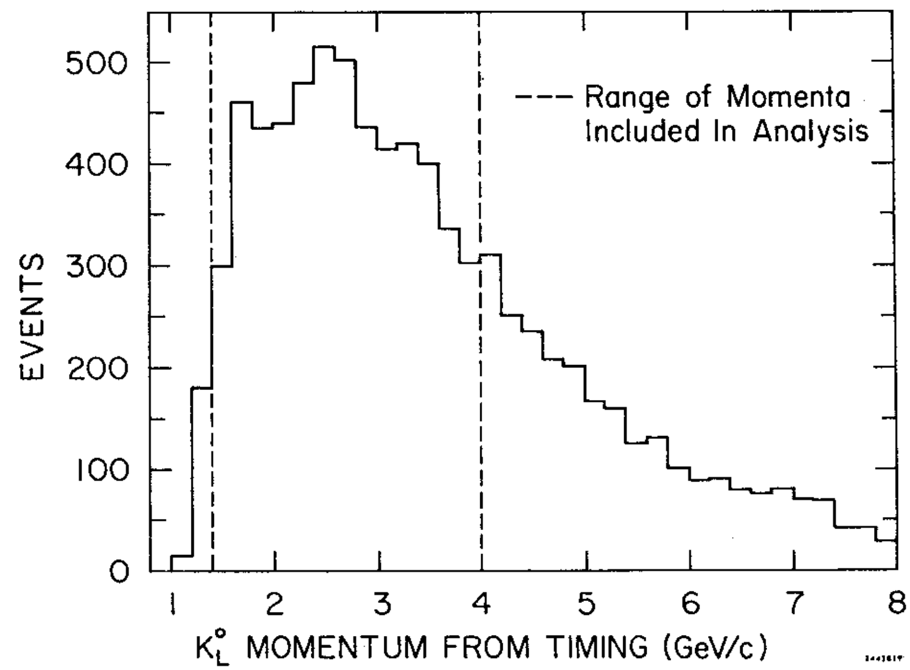

Figure 16 - K_L^0 momentum spectrum.

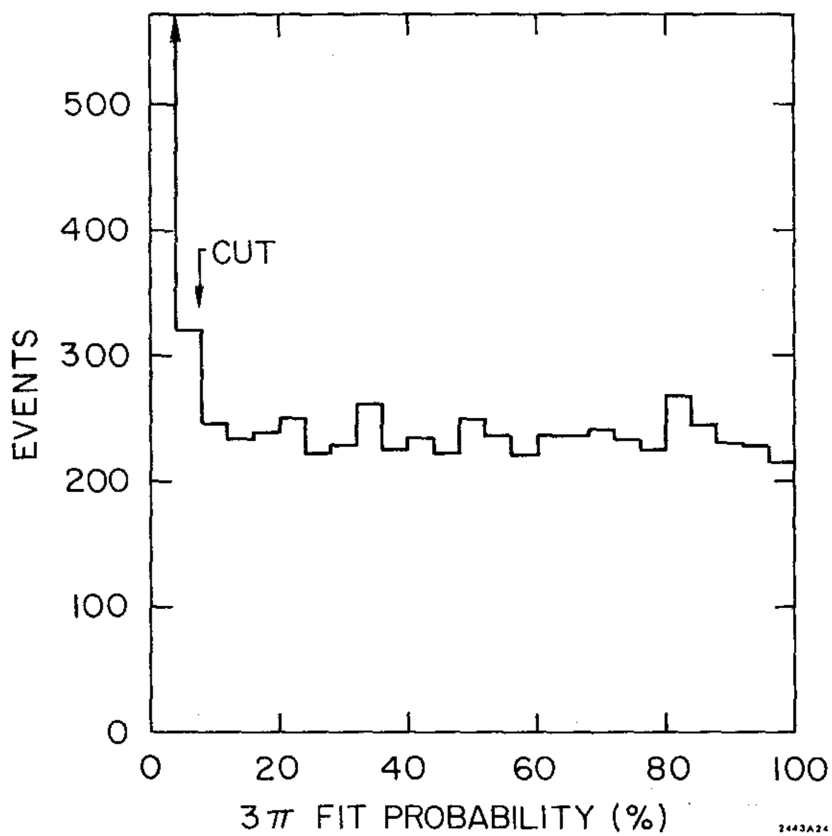

Figure 17 - Kinematic fit probability for the K3pi hypothesis.

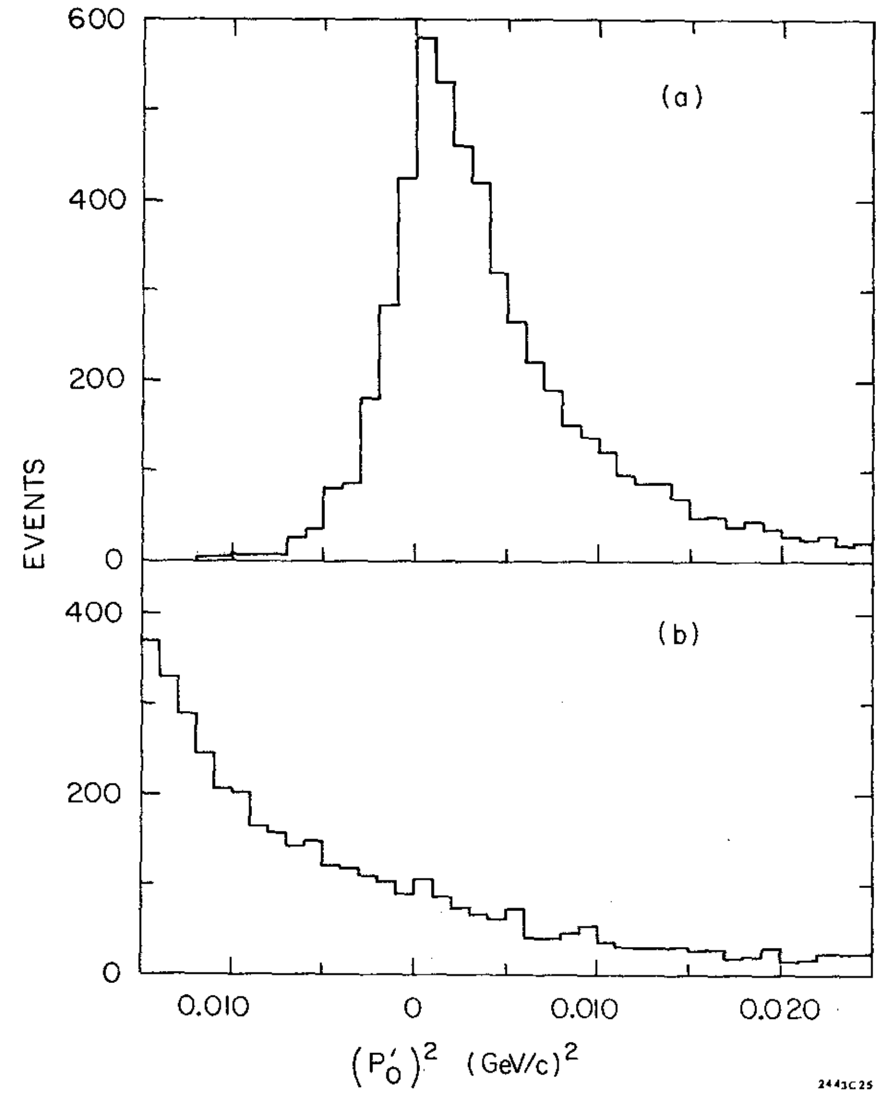

Figure 18 - (P0')² distribution of selected K3pi events and non-K3pi events

CHAPTER V

THE π^0 C.M. KINETIC ENERGY SPECTRUM

Figure 19 shows the spectrum of π^0 c.m. kinetic energy (hereafter called $T(\pi^0)$) for the selected 3 pi fits. The object of the latter stages of analysis was to extract the $T(\pi^0)$ dependence of the square of the decay matrix element from this spectrum. The steps in this procedure were:

a) Each event was weighted for trigger inefficiencies.

b) The effects of finite resolution in moving events from one bin to another were taken into account. The effect of 4-body radiative decays was also considered.

c) The number of events in each bin was corrected for virtual electromagnetic effects.

d) A least squares fit to the corrected spectrum was done to extract the $T(\pi^0)$ dependence.

Each step is fully desribed in the following sections. a), b), and c) were small corrections, but b) and c) depended slightly on the final answer, necessitating iteration. The formulation of step d) was non-linear, so it toc was iterative, regardless of the effect of correcticns.

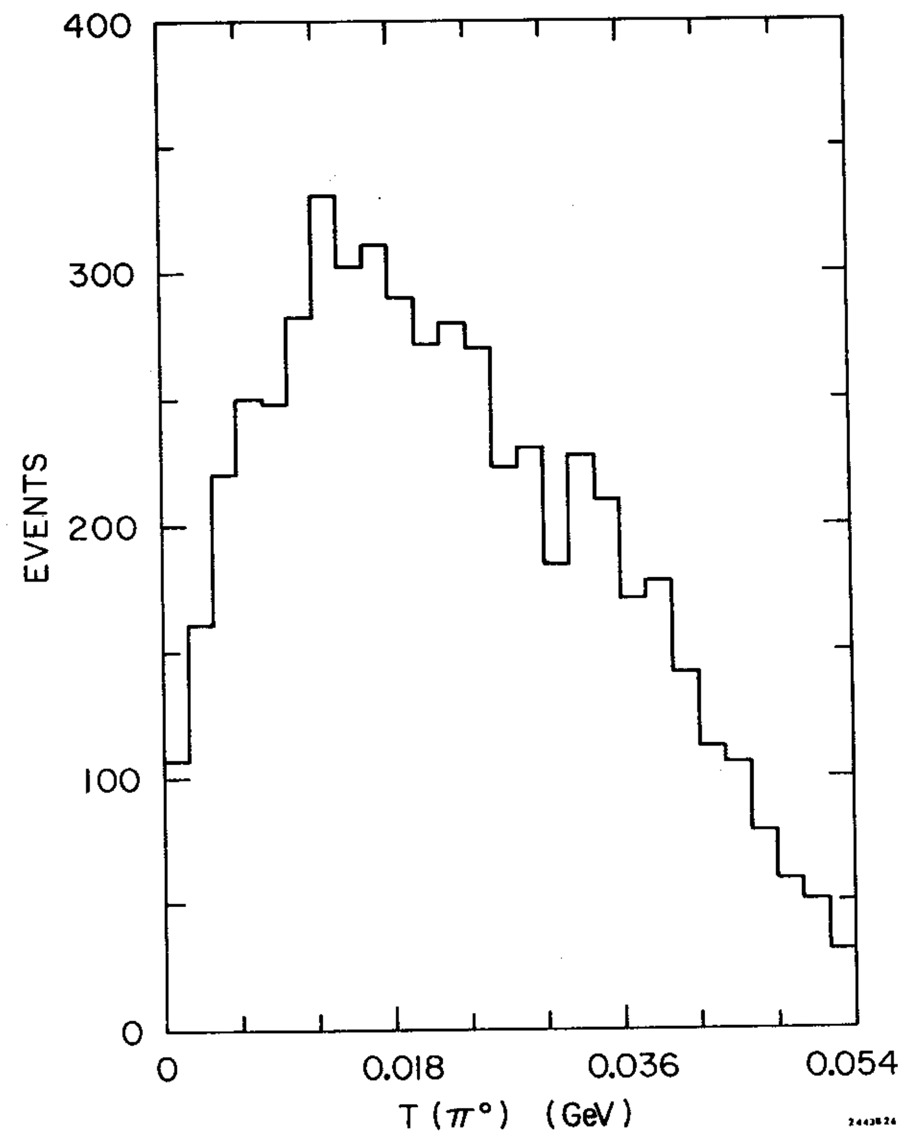

Figure 19 - $T(\pi^0)$ spectrum of selected K3pi events.

TRIGGER CORRECTION

1. Trigger Efficiency

The geometrical efficiency was studied by generating fake (Monte Carlo) events uniformly on the Dalitz plot. The observed beam angles were used, and the charged particle trajectories were integrated through the magnetic field to the trigger counter planes, where it was determined whether the event would have triggered. The events were subsequently weighted in accordance the observed $T(\pi^0)$ spectrum.

10000 events at each of several fixed K_L^0 momenta were generated with a vertex x-coordinate between 0.1 m and 1.1 m. Figure 20 shows the trigger inefficiency as a function of the K_L^0 momentum between 1 GeV/c and 5 GeV/c.

50000 events were generated with the observed K_L^0 spectrum cut off above 6 GeV/c. For K_L^0 momentum between 1.4 GeV/c and 4 GeV/c and vertex x-coordinate between 0.1 m and 1.1 m, the trigger loss was 1.0%.

2. Trigger Weight

The selected 3 pi events were each given a weight to correct for the trigger inefficiency. The calculation of this

weight proceeded as follows. Each event was given many random rotations about the K_L^0 direction. The particle trajectories for each of the rotated configurations were integrated through the magnetic field to the counters and it was decided whether the configuration would have triggered. The weight was then given by the ratio of the number of configurations to the number that would have triggered. The average weight of 1.01 agreed well with the 1% trigger loss observed in the fake events. This correction, though small, was necessary since the non-triggering fake events and the real events with high trigger weight tended to have low $T(\pi^0)$.

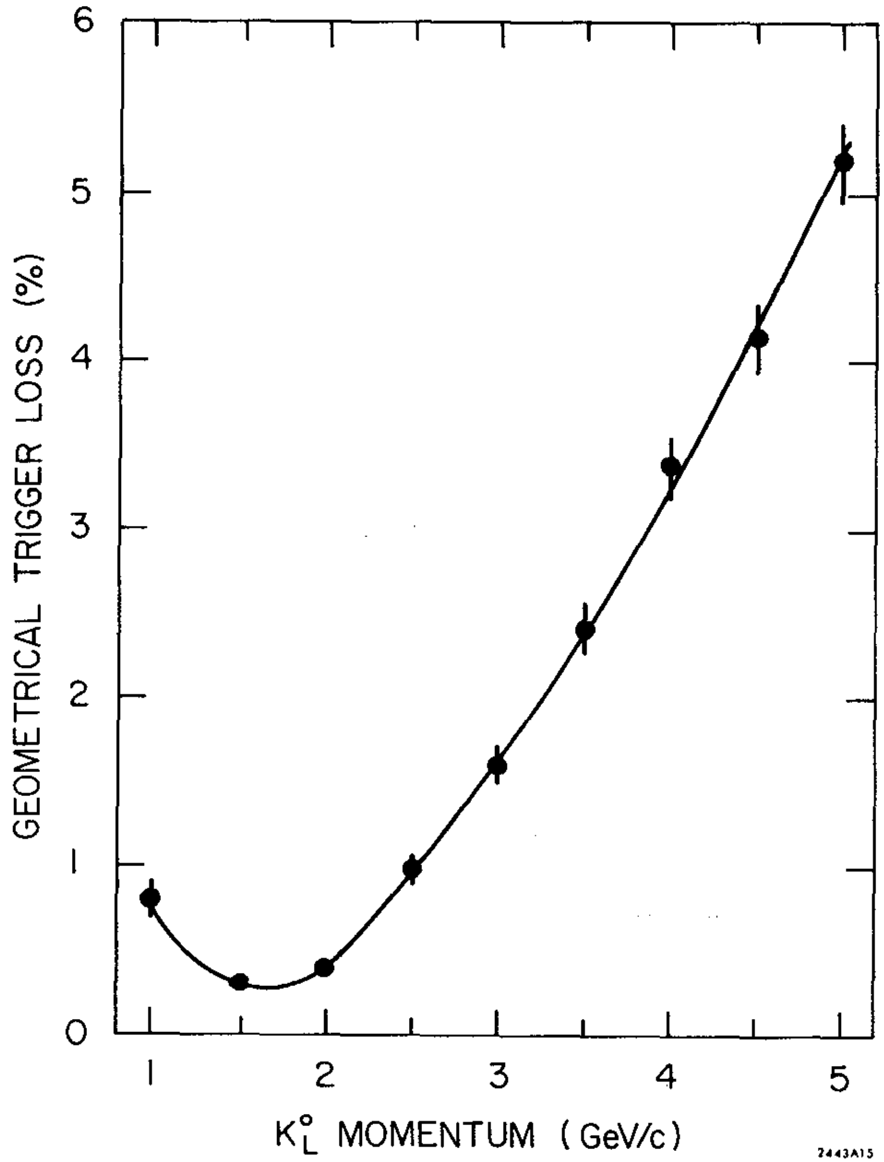

Figure 20 - Trigger loss as a function of K_L^0 momentum.

RESOLUTION CORRECTION

A study of the resolution of the $T(\pi^0)$ measurement was necessary to choose the appropriate bin width for the spectrum and to formulate the correction to the spectrum due to the motion of events from one bin to another.

1. Experimental Resolution

The Monte Carlo events were useful for finding the effects of measurement and reconstruction errors, since the true (generated) value of $T(\pi^0)$ was known. The distribution of the difference between the generated and fitted values of $T(\pi^0)$ had a standard deviation of 2.1 MeV and a mean value of -0.07 MeV. This was compared with the error that was calculated from the fitted variance matrix. The distribution of fitted $T(\pi^0)$ errors gave a typical value of 1.1±0.6 MeV for the Monte Carlo events and 1.4±0.8 MeV for the 3 pi events selected from the real data.

This was all consistent with a typical resolution of 2 MeV for the determination of $T(\pi^0)$. In absence of a resolution correction to the spectrum, a bin width of 5 MeV or even larger would have been dictated, but since a resolution correction was being made, 3 MeV was chosen.

2. Resolution Correction Matrix

The Monte Carlo events were used to construct a matrix that would transform the fitted spectrum (with the bin contents as the elements of a column vector) into the generated spectrum. This matrix would then be applied to the spectrum of the real data.

$$G_i = \sum_j R_{ij} F_j$$

where:

G_i is the number of events in the $i^{\underline{TH}}$ bin of the generated spectrum,

F_j is the number of events in the $j^{\underline{TH}}$ bin of the fitted spectrum, and

R_{ij} is the $ij^{\underline{TH}}$ element of the resolution matrix R.

R_{ij} was given by the fraction of events in the $j^{\underline{TH}}$ fitted bin that had been generated in the $i^{\underline{TH}}$ bin. It should be noted that the resolution matrix depended on the form of the decay spectrum used to weight the events. This was not an important consideration since the resolution correction had a small effect on the slope parameter. Also, since events in a given fitted bin tended to have been generated within one or two bin widths of their final bin, the effect of the decay matrix element was small. In any case, the resolution matrix determination was iterated and the convergence of the procedure was immediate.

Another form of the resolution matrix was tried, namely the inverse of the matrix whose $ij^{\underline{TH}}$ element was the fraction of events generated in the $j^{\underline{TH}}$ bin that ended up in the $i^{\underline{TH}}$ bin after fitting. This inverse matrix had the advantage of being independent of the parameters of the $T(\pi^0)$ spectrum, but it contained rather large negative elements (being the inverse of an all positive matrix). It relied on a delicate cancellation to transform the fitted Monte Carlo spectrum into the generated one, and when it was applied to the real spectrum it amplified the statistical fluctuations to the point of making further analysis hopeless.

RADIATIVE CORRECTIONS

1. Multiplicative Correction

Radiative corrections to order e^2 were necessary due to the processes represented by the Feynman diagrams in figure 21. The infrared divergence in the amplitude for diagrams (b) and (c) is exactly canceled by the low photon energy contribution of diagram (d). The treatment of the 4-body final state was broken into two parts which were quite different.

The rate for very low energy photons (up to 0.05 MeV which was much less than the experimental resolution) was lumped together with the virtual processes (b) and (c). This resulted in a net correction which could be applied on a bin-by-bin or on event-by-event basis[22]. This correction ranged from about 2% for $T(\pi^0)=0$ to about 10% for $T(\pi^0)=53$ MeV The correction diverged for $T(\pi^0)=53.86$ MeV, the kinematic maximum, since this corresponded to zero relative velocity between the two charged pions. The bulk of the variation was due to the coulomb (inner bremsstrahlung) term.

2. 4-body Radiative Decays

Approximately 30000 $K^0_L \longrightarrow \pi^+\pi^-\pi^0\gamma$ decays were generated

in 4-body phase space according to the matrix element of reference 23. They were then run through the geometry and kinematic fitting programs. The 3 pi fit probability showed a low probability spike with 10% of the events below 1% probability and 21% below 8%. The 79% of the 4-body decays with an acceptable 3 pi fit were examined in detail and used for the correction described below.

The fitted value of $T(\pi^0)$ was on the average 1.3±3.3 MeV higher than the generated value. This was expected since the value of $T(\pi^0)$ calculated from the invariant mass of the π^+ and π^- gave in fact the total missing neutral energy, namely $T(\pi^0) + E(\gamma)$. The average photon energy was 2.2 MeV and the effect of the timing information in the 1C fit was to "take back" about 40% of the extra kinetic energy that had been wrongly attributed to the π^0.

Although radiative decays with a photon energy above 0.05 MeV were at the 1% level, their effect was correctable. This was accomplished by adding the radiative event sample in with the 3 pi Monte Carlo events (weighted to reflect the relative branching ratio) before calculating the resolution matrix described in a previous section. The resolution matrix without the radiative decays was retained for comparison.

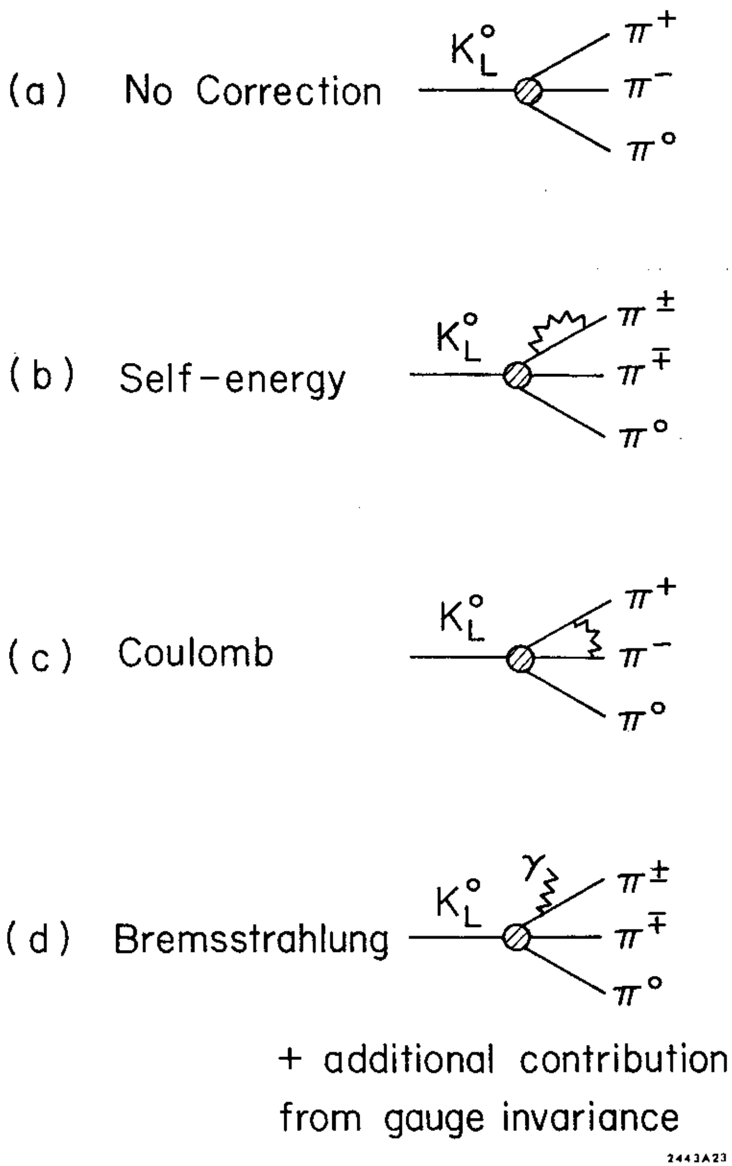

Figure 21 - Feynman diagrams showing radiative corrections to order e^2.

1. Other Modes

We consider here the problem of "events" that were not 3-body charged decays of a K_L^0. Branching ratios cited are from reference 2.

$K_S^0 \longrightarrow \pi^+\pi^-$

K_S^0's originated from regeneration and nuclear interactions mainly in the front wall of the chamber. Their decays were easily distinguishable kinematically, since putting M12=M0 in the formula for $(P0')^2$ gives:

$$(P0')^2 = \frac{-0.98m3^2(1+1.02Pt^2/m3^2)}{(1+Pt^2/M0^2)}$$

$$< -0.98m3^2 \ (=-0.018 \ (GeV/c)^2)$$

These "events" would normally fail the 0C fit (and hence the 1C) but in actual practice were removed by a very gentle $(P0')^2$ cut.

$K_L^0 \longrightarrow \pi^+\pi^-$

The rate of this CP-violating decay is about 0.2% of the rate for all charged decays of the K_L^0. They were removed along with the K_S^0's by the aforementioned $(P0')^2$ cut.

Electron Pairs

π^0's resulted from the decay $K_L^0 \longrightarrow 3\pi^0$ which occurs almost twice as frequently as $K_L^0 \longrightarrow \pi^+\pi^-\pi^0$. 1.17% of the π^0's decay to γe^+e^- with the rest going to two gammas. Gammas converting in the front window of the chamber or in the central electrode mesh were removed by the standard fiducial volume cut (see figure 22), but electron pairs from conversion in the gas or from the internal conversion (Dalitz pairs) remained. Since the pairs tended to be of low momentum (having on the average 1/6 the K_L^0 momentum), they had low total transverse momentum. The invariant mass assuming both to be pions was also low. While many of the pairs thus simulated physical 3 pi decays, the 1C fit eliminated virtually all of them. This was confirmed by an examination of the scanning information.

$\Lambda^0 \longrightarrow p\pi^-$

Λ^0's originating from nuclear interactions in the front window of the chamber were partially removed by the fiducial volume cut, since their $c\tau$ is only 7.73 cm. A noticeable signal persisted however (see figure 23) until the gentle $(PO')^2$ cut was made, at which point the signal vanished. That this should be so was best seen from the Monte Carlo studies which showed that only 2-3% of the Λ^0's survive the $(PO')^2$ cut. The few survivors could be expected to fail the 1C fit.

Nuclear Interactions

Nuclear interactions in the gas of the chamber's sensitive

volume were characterized by a large invariant mass and were removed by the $(PO')^2$ cut. In any case they would have failed the 1C fit.

2. Accidental Triggers

An estimate of the rate of accidental triggers can be made using the fact that there were approximately 50 machine pulses per trigger and approximately 4.5 triggers per V, for a rate of 1 V per 225 pulses. Thus there was a 1/225 chance of an accidental V's occurring in a given triggering pulse. For the V to have shown up in the picture, it must have occurred within 0.8 μs of the trigger (the time delay for the chamber to fire). Averaging the available time over the 1.6 μs pulse length gives a probability of (.6/1.6)/225 or 1/600 for the accidental V to have shown up in the picture. From this it can be seen that about (3.5/600) or 0.6% of the observed events were in fact accidental V's with a non-V trigger, and that (1/600) or 0.2% of the observed events had two V's in the frame. The actual number of double V's observed was about 1% of the total number of V's, which can be explained by the known neutron flux[21] and the cross sections for associated production in the anti counters and front wall of the chamber.

To study the effect of the accidental contamination, a tape was generated where the timing ADC record for each event was taken from the next non-V trigger in the data. The events were run through the kinematic fit with this spurious timing, and about 3.5% were found to give an acceptable 3 pi fit. Normalizing for the 3 pi branching ratio gave a net .1% contamination of the 3 pi sample due to accidental V's. As well as being a numerically small source of contamination, accidentals were found to be relatively bias-free. The slope parameter extracted from the "accidental" events with a good 3 pi fit was consistent with that obtained from the regular 3 pi sample. The reason for this is that the 1C fit with spurious timing had the effect of rejecting about 80% of all events, and crudely selecting 3 pi decays from the remaining 20% by a 0C fit. The fitted value of $T(\pi^0)$ was left more or less intact, since it depended mainly on the measured invariant mass of the charged particles.

3. Backward Gammas

The concern here is that gamma rays from the π^0 could go backward in the lab, convert in the chamber front wall or anti counters, and veto the event. A Monte Carlo study of 3 pi decays showed that approximately 0.8% of the events had a backward gamma ray that could hit the anti counters. Allowing a 2% conversion probability gives a loss of 0.02% by this mechanism. The bias due to this loss is completely negligible, since the events with a backward gamma ray had

the same $T(\pi^0)$ spectrum as the rest of the generated sample.

4. Counter Inefficiency

Events in which both particles hit the trigger counters were used to study the counter efficiencies. The A counters were found to be virtually 100% efficient, but an overall 2% loss was found in the B counters. This was expected since the B counters were behind the lead oxide plates. In fact the losses were confined to track types 0 (nothing comes out) and 4 (large angle scatter). Since 15% of the events had only one particle hitting the trigger counters, the counter inefficiency resulted in a net loss of 0.3%. A Monte Carlo study showed that the slope parameter extracted from these events was about 7% higher than that of the entire sample.

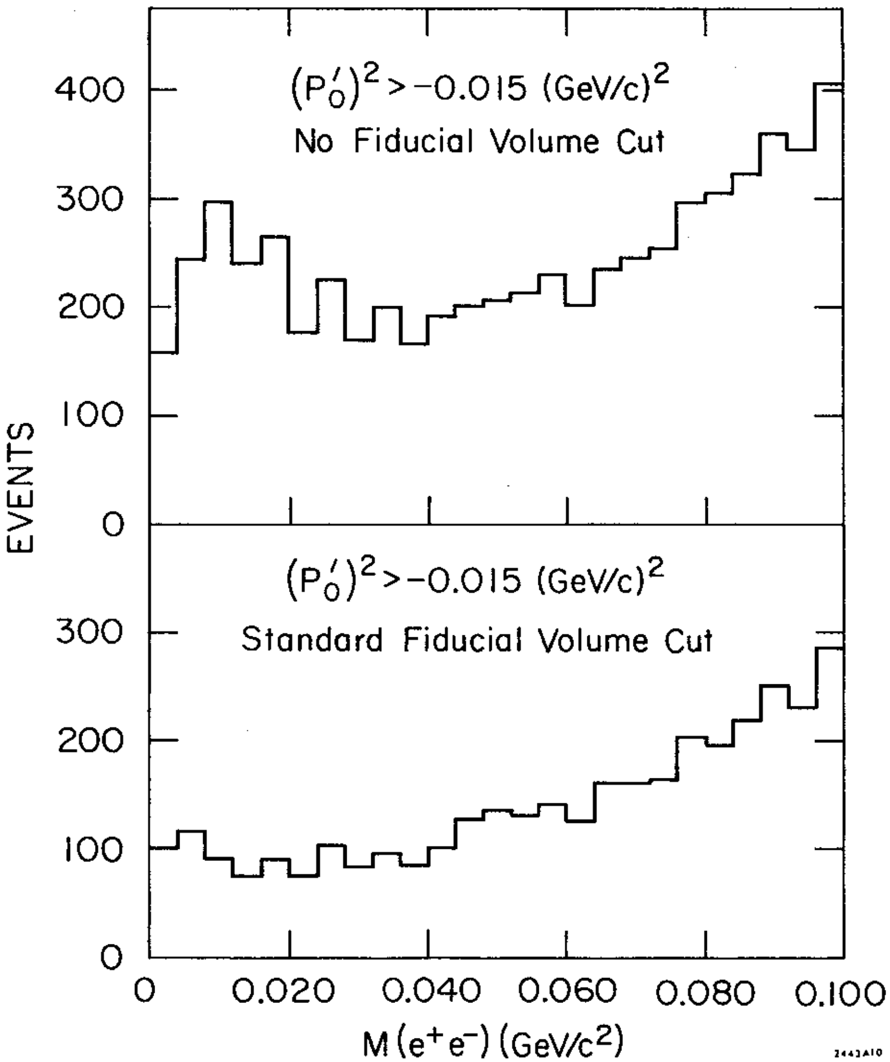

Figure 22 - Invariant mass spectrum assuming e^+e^-.

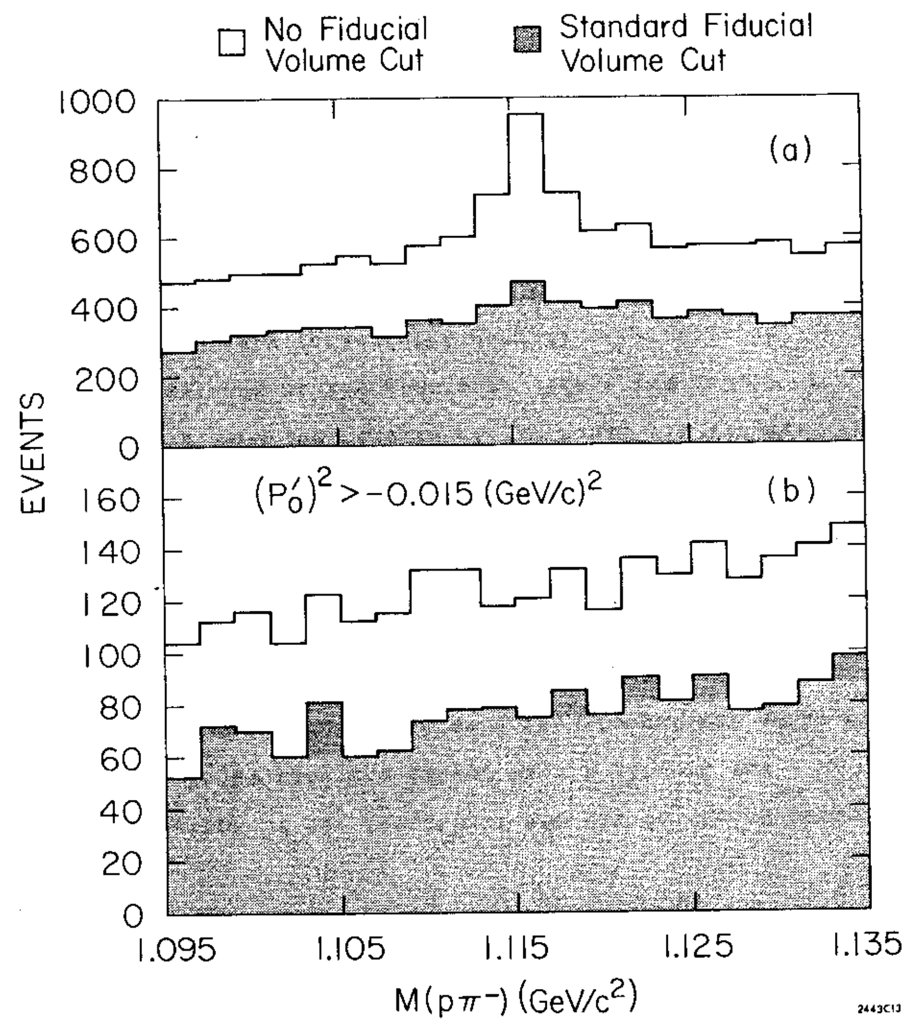

Figure 23 - Invariant mass spectrum assuming $p\pi^-$.

LEAST SQUARES FIT TO THE SPECTRUM

1. Formulation of the Fit

The least squares fit described below was done to the uncorrected $T(\pi^0)$ spectrum, to the spectrum with the corrections applied individually, and to the fully corrected spectrum. The event samples chosen by all three of the selection criteria discussed in the chapter on event selection were analyzed. The errors on the bin contents were evaluated at the expected values, so the χ^2 to be minimized was given by:

$$\chi^2 = \sum_i (n(i) - \int_{\Delta_i} |M|^2 d\phi)^2 / \int_{\Delta_i} |M|^2 d\phi$$

where:

$n(i)$ is the content of the i^{TH} bin,

M is the matrix element expressed as a function of $T(\pi^0)$ and the parameters to be extracted,

$d\phi$ is the phase space element, and

the integral is over the phase space available for the i^{TH} bin in $T(\pi^0)$.

Three forms for $|M|^2$ were tried:

$|M|^2 = a(1+bt)$ (linear spectrum)

$|M|^2 = a'(1+b't)^2$ (linear matrix element)

$|M|^2 = a''(1+b''t+c''t^2)$ (quadratic spectrum)

where:

a, b, a', b', a", b", and c" are the parameters to be extracted,

$t = (2T(\pi^0)-T3max)/T3max$, and

$T3max = 53.86$ MeV is the maximum allowed value of $T(\pi^0)$.

2. Results of the Fit

An examination of the results of the fit to the uncorrected spectrum showed that the linear matrix element was preferred. The corrections were then formulated using the values of a' and b' obtained, the parameters for the corrected spectrum were extracted, and the corrections reformulated in terms of the new parameters. The newly corrected spectrum was then fitted, and since the parameters did not change perceptibly, the process was stopped. Tables 6, 7, and 8 show the results of the final fit for the three parametrizations of the spectrum. Since the values of a, a', and a" merely reflect the overall normalization, they are not shown. The errors quoted in the tables are statistical only.

Table 6

Extracted Parameters for Linear Spectrum
$|M|^2 = a(1+bt)$

	3 pi fit the best	all good 3 pi fits	good 3 pi fit only
uncorrected b	-0.767±0.021	-0.767±0.021	-0.771±0.021
probability	0.8%	1.0%	0.3%
trigger correction b	-0.772±0.021	-0.772±0.021	-0.775±0.021
probability	0.5%	0.7%	0.2%
resolution correction b	-0.768±0.021	-0.768±0.021	-0.772±0.021
probability	6.7%	7.8%	2.9%
resolution & radiative corrections b	-0.787±0.021	-0.787±0.021	-0.791±0.021
probability	10.2%	11.8%	4.8%
all corrections b	-0.792±0.021	-0.792±0.021	-0.795±0.021
probability	7.4%	8.8%	3.3%

Table 7

Extracted Parameters for Linear Matrix Element
$|M|^2 = a'(1+b't)^2$

	3 pi fit the best	all good 3 pi fits	good 3 pi fit only
uncorrected b'	-0.425±0.014	-0.424±0.014	-0.428±0.014
probability	6.8%	5.1%	4.4%
trigger correction b'	-0.428±0.014	-0.428±0.014	-0.432±0.014
probability	6.5%	4.8%	4.0%
resolution correction b'	-0.425±0.014	-0.425±0.014	-0.429±0.014
probability	44.6%	36.2%	35.3%
resolution & radiative corrections b'	-0.439±0.014	-0.438±0.014	-0.442±0.014
probability	56.1%	46.8%	47.0%
all corrections b'	-0.443±0.014	-0.442±0.014	-0.446±0.014
probability	54.2%	45.2%	44.4%

Table 8

Extracted Parameters for Quadratic Spectrum
$|M|^2 = a''(1+b''t+c''t^2)$

	3 pi fit the best	all good 3 pi fits	good 3 pi fit only
uncorrected			
b"	-0.832±0.033	-0.826±0.032	-0.844±0.033
c"	0.134±0.052	0.119±0.052	0.148±0.054
probability	5.6%	4.7%	3.3%
trigger correction			
b"	-0.841±0.033	-0.835±0.032	-0.852±0.033
c"	0.141±0.052	0.126±0.051	0.155±0.053
probability	5.1%	4.3%	2.9%
resolution correction			
b"	-0.839±0.033	-0.833±0.033	-0.851±0.033
c"	0.148±0.053	0.133±0.052	0.162±0.054
probability	39.5%	33.8%	29.6%
resolution & radiative corrections			
b"	-0.862±0.034	-0.856±0.033	-0.873±0.034
c"	0.152±0.054	0.137±0.053	0.166±0.055
probability	52.5%	46.2%	41.4%
all corrections			
b"	-0.871±0.033	-0.865±0.033	-0.881±0.034
c"	0.158±0.053	0.145±0.052	0.172±0.054
probability	49.8%	43.8%	38.5%

RESULTS

As is shown in Tables 6,7, and 8, the differences in the extracted parameters due to different event selection criteria were well within the statistical errors. The exclusion of the 91 events with a better semileptonic fit was indicated by the fact that this small sample had a significant fraction of tracks with electron-like scan codes. No such effect was found in the other 130 events with a good semileptonic fit, so there was no logical reason to exclude them.

Since the fit to a quadratic spectrum was slightly worse than that to a linear matrix element, only the linear spectrum and linear matrix element will be considered.

1. Systematic Errors

Possible contamination or loss due to the 1C fit was at the 2% level (an upper limit of 91 events lost or 130 events contaminating). The maximum effect on the slope parameter was 1%. Other sources of contamination and loss were a few tenths of a percent at most and were found to have negligible effect on the slope parameter. The corrections applied to the spectrum resulted in a 3-4% increase in the slope parameter. An error in the corrections of 25%, which is a pessimistic estimate, would have resulted in a 1% error in the slope parameter.

Thus a net 2% was felt to be a very conservative upper limit of the possible systematic error on the slope parameter. The correct way to combine the statistical and systematic errors was unclear, so they were not combined. The errors quoted below are statistical only. The quoted error on the linear spectrum slope parameter has not been scaled by 1.3 to reflect $\sqrt{\chi^2/DF}$ for that fit. The factor for the linear matrix element would be 1.0 .

2. Linear Spectrum

This is the most common way of parametrizing the data, but our results show that it is not as good as a linear matrix element. The reason for its persistence is that early experiments got a smaller (in absolute value) slope and the difference was not of importance. Our result in terms of b is:

$$b = -0.792 \pm 0.021$$

Common practice expresses the slope in terms of g or σ_o where:

$$|M|^2 \sim 1 + g(s3-s0)/m(\pi^+)^2$$

$$|M|^2 \sim 1 + 2\sigma_o M(K_L^0)(2T(\pi^0)-T3max)/m(\pi^+)^2$$

In terms of these parameters our results are:

$$g = 0.630 \pm 0.017$$

$$\sigma_o = -0.287 \pm 0.008$$

3. Linear Matrix Element

Our result in terms of b' is:

$$b' = -0.443 \pm 0.014$$

If g' and σ_o' are used to express the matrix element as:

$$|M| \sim 1 + g'(s3-s0)/2m(\pi^+)^2$$

$$|M| \sim 1 + \sigma_o' M(K_L^0)(2T(\pi^0)-T3max)/m(\pi^+)^2$$

we have:

$$g' = 0.714 \pm 0.023$$

$$\sigma_o' = -0.321 \pm 0.010$$

Figure 24 shows the corrected $T(\pi^0)$ spectrum divided by phase space. The curve represents the best fit for the linear matrix element squared.

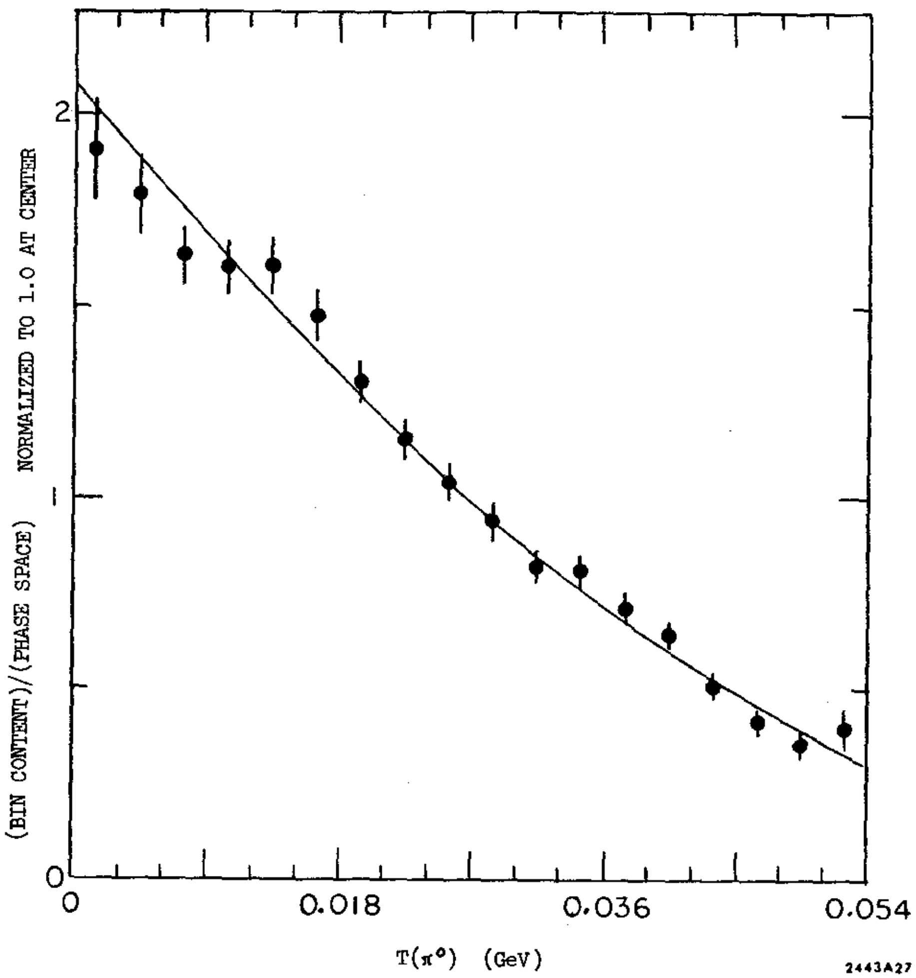

Figure 24 - Decay matrix element squared extracted from the corrected spectrum as a function of T(π^0)

CHAPTER VI

CONCLUSIONS

INTERPRETATION

1. Comparison with Others' Results

The $T(\pi^0)$ spectrum has been studied in many experiments and the latest compilation[2] gives a world average value of 0.610 ± 0.021 for the slope parameter g. Unfortunately, a comparison of this number with our result can be very misleading for two main reasons.

The compilation consists of seventeen values. Of the eight most recent measurements[24-31], four[24-27] did the fit in terms of a linear spectrum only, and three others[28-30] allowed quadratic dependence in the spectrum but found it consistent with zero. This qualitative feature is in disagreement with our findings. Since our data clearly indicates the presence of a quadratic term in the spectrum, our value of g is not terribly relevant. Our value of g' (0.714 ± 0.023) is the slope parameter of importance, and it is significantly higher than the world average of g. It may be noted that a recent high statistics experiment[32] not included in the compilation has also found substantial deviation from a linear spectrum.

Because of the small Q of the 3 pi decay, it is natural to try to expand the matrix element in a power series of the kinematic variables. Since the final state interactions are

presumably small[33], the matrix element is expected to be nearly real. The simplest non-constant matrix element would be linear in $T(\pi^0)$, and our result is consistent with this. Our analysis in terms of a quadratic spectrum indicates that the imaginary part of the slope parameter is consistent with zero (assuming a complex linear matrix element), and the fit assuming a real linear matrix element actually has a slightly higher probability. A linear spectrum would have been somewhat of a surprise since it would have demanded a very specific relation between the linear and quadratic coefficients in the matrix element.

Also of importance in discounting the significance of a comparison of our results with the world average is the fact that the agreement among the seventeen values of g is extremely poor. The large χ^2 (69.1 for 16 degrees of freedom) indicates that it is not really meaningful to average the results. It seems clear that at least some of the experiments suffered from significant systematic errors. Without singling any of the individual experiments out, it is nevertheless helpful to consider some of the problems that could be responsible for the contradictory results.

Many experiments have had a geometrical efficiency which was low and non-uniform over the Dalitz plot. It goes without saying that the large corrections necessary to yield a spectrum from which the matrix element can be extracted would not have to be very much in error to give erroneous final results. As has been mentioned earlier, the separation of the decay modes is critical. Virtually all of the experiments to date have not had a constrained kinematic fit. The lack of such a constraint makes the separation more difficult. Many experiments have not taken into account the effects of resolution on the $T(\pi^0)$ spectrum. In cases where the resolution is poor, the resultant defotmation of the spectrum could severely affect the slope parameter determination. Also of importance is the fact that the data from some experiments have not been corrected for electromagnetic effects. As can be seen from Tables 6-8, radiative corrections are not negligible.

2. The $\Delta I=1/2$ Rule

As was previously described, a comparison of the matrix element slope parameters for the 3 pi decays of the K^0_L and K^+ leads to certain conclusions regarding the isospin transitions involved in the decays.

The world averages of the slope parameters for K^+ decays are[2]:

$$g(++-) = -0.214 \pm 0.004$$

$$g(00+) = 0.522 \pm 0.020$$

The experimental situation for the the K^+ slopes is a little better than that for the K^0_L since the compiled values of $g(++-)$ and $g(00+)$ are in better agreement with each other. This is partly due to the smaller number of individual experiments, and in the case of $g(00+)$, to the relatively large errors. The experiments measuring $g(00+)$ have all had fairly low statistics. There are experimental difficulties in detecting the gammas from the π^0 decays, and the existence of some high values in the compilation may be taken as an indication that the final word regarding this mode has yet to be said.

The parametrization in terms of spectrum slope is unfortunate since the matrix element slope is what is really wanted. The distinction is not large for $g(++-)$ since its magnitude is small, but the quoted value of $g(00+)$ is presumably somewhat lower than the desired matrix element slope. While the computations done below are very sensitive to the values of the slopes and should use matrix element slopes, $g(++-)$ and $g(00+)$ will be used unchanged (there is no choice). As for the K^0_L slope, both $g(+-0)$ and $g'(+-0)$ will be considered, as well as the world average of $g(+-0)$.

The notation in the discussion that follows is the same as that used in Chapter I. The slope parameters $\sigma(++-)$, etc. differ from $g(++-)$, etc by a constant factor $2m(\pi^+)^2$, but the factor cancels out in the computation.

A study of the reduced rates (see reference 2, p. 193) shows no real evidence for I=3 in the final state, so $a^+(3,S)$ and $a^0(3,S)$ will be set to zero. Expressing the slope parameters in terms of the irreducible matrix elements gives:

$$\frac{g(+-0) + g(++-) - g(00+)/2}{g(+-0)} = \frac{3(\delta - \epsilon)}{2(1 - \epsilon/2)(1 + \delta)}$$

where:

$\epsilon = \lambda^{(3)}/\lambda^{(1)}$ is the ratio of the $\Delta I=3/2$ to $\Delta I=1/2$ contribution to the I=1 symmetric final state, and

$\delta = \mu^{(3)}/\mu^{(1)}$ is the analogous quantity for the I=1 non-symmetric state.

Thus ϵ is a measure of the violation of the $\Delta I=1/2$ rule for the symmetric waves; δ for the non-symmetric. ϵ can be determined from the reduced rates[33] and has been found to have the value -0.064 ± 0.008 . Depending on the value of $g(+-0)$ used this leads to the following values for δ:

$\delta = 0.105 \pm 0.031$ for $g(+-0) = 0.610$ (world average)
$\delta = 0.126 \pm 0.026$ for $g(+-0) = 0.630$ (our value for g)
$\delta = 0.216 \pm 0.026$ for $g(+-0) = 0.714$ (our value for g')

Since the value of $g(00+)$ can be considered suspect, it is of interest to calculate δ without using it directly. This can be done as current algebra makes the prediction[34]:

$g(+-0) = g(00+)$

Calculating as above:

$\delta = 0.043 \pm 0.015$ for $g(+-0) = 0.610$ (world average)
$\delta = 0.052 \pm 0.013$ for $g(+-0) = 0.630$ (our value for g)
$\delta = 0.086 \pm 0.013$ for $g(+-0) = 0.714$ (our value for g')

3. Conclusions

It seems clear that the $\Delta I=1/2$ rule is violated at the level of several percent. The admixture of $\Delta I=3/2$ for the non-symmetric final state (δ) is quite sensitive to the particular values of the slopes used, but is in the 5%-20% range and has the opposite sign to the $\Delta I=3/2$ admixture for the symmetric state (ϵ).

The precise value of δ should not be taken too seriously until the slope parameter $g(00+)$ is better determined. $g(00+)$ is also of interest as a check of current algebra as mentioned above, and one would hope that a definitive measurement might be forthcoming in the near future.

There are also theoretical difficulties. The general attitude implicit in the whole discussion has been that the effect of final state strong interactions is small, and that the observed structure is an intrinsic property of the weak interaction. Quite the opposite viewpoint, namely that final state interactions of the pions are entirely responsible for the observed deviations from phase space, has been taken by several authors[35-38] with some degree of success. It is beyond the scope of this paper to address such questions in detail, except perhaps to note that the relative success of current algebra predictions tends to favor the viewpoint that the weak interaction itself is mainly responsible for the observed slopes.

We have performed a reliable measurement of the matrix element slope parameter. On this basis certain conclusions have been drawn regarding the $\Delta I=1/2$ rule. Clearly such an interpretation suffers from present theoretical ambiguities which are in need of work.

RETROSPECTIVE

No matter how well designed and executed an experiment is, there are always certain things that one would do differently if one were performing the experiment again. The purpose of this short section is to outline some of the features that might be changed were the experiment to be redone.

The resolution on the beam angles might have been improved had a shorter, more point-like target been used. Helium or vacuum along the entire flight path would have cut down the scattering of the K^0_L's. The flux of low energy K^0_L's might have been increased had a higher energy electron beam been used with a radiation length of copper before the target.

The quality of the timing information would have been slightly better had the A and B counters been on the decay vertex side of the lead oxide plates and the C and D counters directly behind the plates. The chamber could then have been rectangular which would have allowed better track measurement behind the plates (important in analyzing the semileptonic modes). This was not done because of the difficulty in getting the counter light pipes out of the chamber in such a geometrical configuration, but whether it was truly impossible is not known.

Tilted optic axes would certainly have been used to reduce vignetting in the downstream view and optical distortions in all three views. In fact this has been done on all subsequent streamer chamber experiments.

The effectiveness of the scanning information might have been increased had the scan codes been formulated differently. This again is likely to be more important in the semileptonic analysis. Measuring all five fiducials rather than three probably would have made a slight improvement in the overall quality of the track measurements.

REFERENCES

1. A. Pais, (M. Gell-Mann), Proceedings of the Fifth Annual Rochester Conference (1955).

2. Particle Data Group, Physics Letters 50B, no.1 (1974).

3. J. Bernstein, "Elementary Particles and Their Currents", p. 286, W. H. Freeman and Co. (1968).

4. A. Sirlin, "Lectures on Weak Interactions", p. 180, 1969 Summer School Centro de Investigacion y de Estudios Avanzados del I. P. N.

5. R. E. Marshak, Riazuddin, and C. P. Ryan, "Theory of Weak Interactions in Particle Physics", p. 605, Wiley-Interscience (1969).

6. C. G. Callen and S. B. Treiman, Phys. Rev. Letters 16, 153 (1966).

7. R. H. Dalitz, Physical Society of London Proceedings, A69, 527 (1956).
   R. H. Dalitz, Rev. Mod. Phys. 31, 823 (1959).

8. S. Weinberg, Phys. Rev. Letters 4, 87 (1960).

9. G. Barton, C. Kacser, and S. P. Rosen, Phys. Rev. 130, 783 (1963).

10. M. E. Rose, "Elementary Theory of Angular Momentum", p. 85, John Wiley & Sons, Inc.

11. F. Bulos, A. Odian, F. Villa and D. Yount, "Streamer Chamber Development", SLAC Report 74 (1967).

12. A. Odian, private communication.

13. B. Bertolucci, "A Digital Time Sequence Generator", SLAC-TN-70-10.

14. "Kodak Data for Aerial Photography" (Second Edition), p. 13, Eastman Kodak Co., Rochester, NY.

15. R. H. Dalitz, Phys. Rev. 94, 1046 (1954).

16. W. R. Frazer, "Elementary Particles", p. 71, Prentice-Hall, Inc.

17. F. T. Solmitz, Ann. Rev. Nucl. Sci. 14, 375 (1964).

18. J. P. Berge, F. T. Solmitz, and H. D. Taft, Rev. Sci. Instr. 32, 538 (1961).

19. D. E. C. Fries, "Filmplane Reconstruction of Trajectories in a Nonuniform Magnetic Field: the Computer Program Sybil", SLAC Report 103 (1969).

20. J. C. H. Park, "FIT73 - A Kinematic Fitting Routine", to be published.
A predecessor of FIT73 was FIT70, which is described in J. C. H. Park, "FIT70 - A Kinematic Fitting Routine", SLAC Report 150 (1972).

21. G. W. Brandenburg, A. D. Brody, W. B. Johnson, J. S. Loos, G. J. Luste, J. A. J. Matthews, K. Moriyasu, B. C. Shen, W. M. Smart, F. C. Winkelman, and R. J. Yamartino, Phys. Rev. 7D, 708 (1973).

22. The Fortran code was supplied by R. L. Messner (Univ. of Colorado) and was based on the unpublished calculations of Jack Smith (SUNY Stony Brook). The result agreed with that of Neveu and Scherk in the limit of very low photon energy, but handled the higher energies more correctly.
A. Neveu and J. Scherk, Phys. Letters 27B, 384 (1968).

23. R. Ferrari and M. Rosa-Clot, Nuovo Cimento 56A, 582 (1968).

24. F. James, L. Montanet, E. Paul, P. Saetre, D. M. Sendall, P. Bertranet, G. Burgun, E. Lesquoy, A. Muller, E. Pauli, S. Zylberajch, and O. Skjeggestad, Nucl. Phys. B49, 1 (1972).

25. W. Krenz, H. W. K. Hopkins, G. R. Evans, J. Muir, and K. J. Peach, Nuovo Cimento Letters 4, 213 (1972).

26. M. Metcalf, G. Neuhofer, F. Niebergall, M. Regler, H. Stier, K. Winter, J. J. Aubert, X. de Bouard, V. Lepeltier, L. Massonet, H. Pessard, M. Vivargent, T. R. Willitts, M. Yvert, W. Bartl, and M. Steuer, Physics Letters 40B, 703 (1972).

27. G. Alexander, O. Benary, I. Borowitz, K. Lande, Y. Oren, I. Stumer, E. Burkhardt, H. Filthuth, A. Putzer, and I. Bar-Nir, Nucl. Phys. B65, 301 (1973).

28. M. G. Albrow, D. Aston, D. P. Barber, L. Bird, R. J. Ellison, C. Halliwell, R. E. H. Jones, A. D. Kanaris, F. K. Loebinger, P. G. Murphy, M. Strong, J. Walters, A. J. Wynroe, D. D. Yovanovic, and R. F. Templeman, Physics Letters 33B, 516 (1970).

29. C. D. Buchanan, D. J. Drickey, F. D. Rudnick, P. F. Shepard, D. R. Stork, H. K. Ticho, C. -Y. Chien, B. Cox, L. Ettlinger, L. Resvanis, R. A. Zdanis,

E. Dally, E. Seppi, and P. Innocenti, Physics Letters 33B, 623 (1970).

30. G. W. Brandenburg, W. B. Johnson, D. W. G. S. Leith, J. S. Loos, J. A. J. Matthews, F. C. Winkelman, and R. J. Yamartino, "A Measurement of the Kmu3/Ke3 Branching Ratio, and the K3pi Decay Parameters", SLAC Report 1212 (1973).

31. R. C. Smith, L. Wang, M. C. Whatley, G. T. Zorn, and J. Hornbostel, Physics Letters 32B, 133 (1970).

32. R. L. Messner, Univ. of Colorado Ph.D. thesis, to be published.

33. M. K. Gaillard, "Some Open Questions in K Decay", Preprint CERN-TH-1693, Talk Presented at the Triangle Meeting on Weak Interactions (1973).

34. C. Bouchiat and Ph. Meyer, Physics Letters 25B, 282 (1967).

35. N. N. Khuri and S. B. Treiman, Phys. Rev. 119, 1115 (1960).

36. G. Barton and C. Kascer, Phys. Rev. Letters 8, 226 (1962).

37. R. N. Chauduri, Phys. Rev. 175, 2066 (1968).

38. D. Greenberg, Phys. Rev. 178, 2190 (1968).